Final Report

DYNAMICS OF PLANKTON POPULATION IN UPWELLING AREAS

Contract No. NAS 5-21784

Karl-Heinz Szekielda
Principal Investigator

Assistant Professor
College of Marine Studies
University of Delaware
Newark, Delaware

TABLE OF CONTENTS

1. INTRODUCTION

The main objective of our study was to demonstrate that ERTS-1 data can be used for locating marine phytoplankton populations in upwelling areas along the Northwest coast of Africa.

Plume-like structures of upwelled water drifting off the coast appear to be a common feature of data taken in the Peru, Oregon, Benguela, Somali, and Canary upwelling areas by various techniques of shipboard surface mapping of nutrients, chlorophyll and temperature, and with airborne and satellite temperature and color sensors. These offshore plumes are of relatively small area, contain sharp gradients of environmental variables, and satisfy our logistic requirements for study of the temperal and spatial behavior of upwelling ecosystems.

The persistence of these quasi-steady state plumes or microstructure of upwelling areas is unknown over time periods greater than one month. Off Peru, during periods of weak upwelling, a series of cold water, high chlorophyll plumes occur along the coast and are associated with very dense schools of anchoveta. In periods of strong upwelling, distinct plumes are not observed and the anchoveta populations are now no longer localized but exhibit a diffuse pattern along the Peruvian coast.

With ERTS-1 data we anticipated that changes in sea color as monitored by the multi-channel scanner (MSS) could be used

to detect chlorophyll gradients and patchiness in the distribution of phytoplankton.

Light penetration in water is affected by plankton, algae, and dissolved and suspended matter. As a result, the composition of backscattered light from below the air-sea interface is determined by the nature of the constituents in the water column. In contrast to the absorption spectrum of chemically-pure chlorophyll in solution, algae suspensions absorb and scatter light more uniformly throughout the visible part of the electromagnetic spectrum. Because of the spectral absorption and scattering properties of plankton, its concentration can be estimated by measuring the spectral backscattered radiance over water.

The radiation from the ocean's surface as measured with an orbiting photometer or spectrometer is primarily a result of incident radiation specularly reflected from the air-sea interface and the upwelling radiation from below the surface. Curran (1972) modelled the atmospheric influence on color ratios remotely sensed from space.

The radiance upwelled from the water column is a function of particles and organisms in the water and dissolved colored organic compounds such as humic acids and pigments in the cells of phytoplankton. If the sunglint has been avoided, the albedo $A_s(\lambda)$ of the ocean's surface may be described by the wavelength-dependent radiance $I(\lambda)$, the irradiance incident on the ocean surface from above.

$$A_s(\lambda) = \frac{\pi I(\lambda)}{F_s(\lambda)}$$

The irradiance $F_s(\lambda)$ is a composite of directly transmitted solar irradiance and the diffuse radiation. The most simple description of the two components can be given by

$$F_s(\lambda) = \mu_o F_t(\lambda) + F_D(\lambda)$$

where $F_s(\lambda)$ represents the irradiance, $\mu_o F_t(\lambda)$ is the directly transmitted solar energy and μ_o is the cosine of the solar zenith angle. $F_D(\lambda)$ is the diffuse incident part of the incoming radiation from space.

Any outgoing radiation from the ocean surface will be influenced by aerosols and molecular constituents. Curran (1972) used for an atmospheric transfer model the optical depth $\Gamma(\lambda)$ which is defined by

$$\Gamma(\lambda) \int_o^\infty = n(z)\, \beta_A(\lambda, z)\, dz.$$

This integration is over altitude z, n(z) is the particle number density and $\beta_A(\lambda, z)$ the volume scattering coefficient.

The number density dn (z,r) of particulates was based on an assumed power law distribution with size parameter v*, the particle radius r in micrometers, the altitude z in kilometers.

$$dn(z,r) = c(z)\, r^{-(v^* + 1)}\, dr$$

The aerosol optical depth is wavelength-dependent. Since Clarke, Ewing and Lorenzen (1970) used color ratios, Curran (cited above) calculated wavelength-dependent properties for different values of v* and came to the conclusion that the optical depth

must be known to an accuracy of $\pm$ 0.01, which makes precise vertical measurements necessary. However, if one assumes that the horizontal values for the aerosol optical density are constant over a certain distance interval, useful information about the postion and the strength of plankton gradients from space can be obtained. This approach was used in interpreting ERTS-1 data for application in our study of plankton blooms and their dynamics.

The highest possible accuracy calculated with the model by Curran (1972) showed that useful estimates of chlorophyll concentration can be made from satellite altitudes. This statement is especially true for strong gradients of plankton in upwelling areas where concentrations of chlorophyll higher than one microgram per liter with maxima up to 40 $\mu g \cdot l^{-1}$ and more can be found.

The multispectral scanner which was carried on ERTS-1 records the radiance from the earth's surface in four spectral bands. The energy was simultaneously recorded between 0.5-0.6, 0.6-0.7, 0.7-0.8, and 0.8-1.1 micrometers. A scan mirror oscillates continuously perpendicular to the spacecraft velocity. The active scanner is from west to east while the passive scan is used to calibrate the optical system. For the detection of the radiance, six lines are collected in each of the four bands. The ground resolution of the scanner is about 90-100 meters; however, objects with a high contrast, such as highways, can still be recognized in the imageries. For our analysis we used the imageries in black and white. In some analysis the original negatives

were used for an enhancement. Although ERTS was not designed for an application in oceanography, it was proved that areas with high plankton concentrations can be monitored with this system.

The photon penetration depth in water decreases as wavelength increases; thus, any response in channel 7 defines a very near surface feature or atmospheric contribution (clouds). This allows the use of channel 7 as a cloud discriminator in judging whether or not the field of view of the MSS is cloud-free.

2. SPECTRAL PROPERTIES OF PLANKTON

In respect to ERTS-1 recordings the maximum energy backscattered from plankton or organisms is covered by the two channels between 0.5 and 0.6 μm and 0.6 to 0.7 μm; however, extremely high concentrations of plankton near the sea surface should be visible in other channels as well.

When monitoring plankton or biomass from high altitudes, we must consider the fact that algae behave more like a suspension than a pure solution of chlorophyll. As a result, solar light will be scattered at the outer shell of the plankton organisms. The absorption of incident irradiance by the cells depends on their outer structure and the optical density inside the cell. Variation in the optical density or the configuration of the cells may change the intensity of backscattered light even if the incident solar irradiance, sun angle, and chlorophyll concentration per unit of volume remain constant. Yentsch (1960) found that the

red absorption band of chlorophyll has little influence on water color. This means that the signal obtained with the MSS in channels 5 and 6 would record primarily the effect of backscattered light from the organisms.

The intensity of backscattered light caused by plankton and dissolved matter from the ocean as a function of wavelength is given in Fig. 1. Gulf Stream water was used as a reference water assuming that the chlorophyll concentration of less than 0.02 $\mu g \cdot l^{-1}$ does not change significantly the backscattered light compared to pure water. It was assumed, for the interpretation of the different spectra, that sky conditions, sun angle, and sea state were the same over both sites. The spectrum in Fig. 1 is the difference in energy between the spectrum obtained in near-coastal water and the spectrum recorded over the Gulf Stream.

If both water masses had the same optical characteristics and oceanic conditions, the energy difference in both spectra should be equal to zero. Any differences between the two signals would thus be caused by dissolved and/or particulate matter in the sea. If chlorophyll affected the backscattered light by its absorption properties in the shorter wavelengths, we would expect differences near the absorption bands of chlorophyll.

Chlorophylls have two main absorption maxima in the visible region of the electromagnetic spectrum. The main absorption peaks for pure chlorophyll a are at 0.446 μm and 0.663 μm. However, the naturally occurring chlorophyll a types in plants have spectra

with peaks near 0.673 and 0.683 μm. Other forms show maxima near 0.690 and 0.710 μm.

The spectrum in Fig. 1 shows that the first and the second absorption bands of chlorophyll have only a minor influence on the total backscattered light. Strong absorption appears at about 0.72 μm, but the maximum of backscattered light appears at 0.58 μm. Considering only the portion between the second absorption band and the near-infrared, it can be seen that only a linear decrease of backscattered light appears. This is an indication that in addition to the absorption of light by chlorophyll, backscattered light from the organisms themselves contributes to the total backscattered energy. Thus, the size and concentration of particles or marine organisms seem to be the important contributors to the changes in backscattered light intensity as measured in the ERTS-1 channels. The scattering intensity of suspended particles is proportional to λ^{-n} where λ is the wavelength and n the Rayleigh value which may vary from 4 for pure water to 0 at high turbidity. In other words, the intensity of backscattered light increases with particle concentration. This shows the important influence of particles without chlorophyll on the backscattered light from below the sea surface.

It must be recognized that backscattered light from below the surface is most affected by plankton in the blue region. This is supported by data published by Clarke, et al. (1970). Representative spectra obtained from their aircraft missions over water with different plankton concentrations are shown in Figure 2,

together with the relative spectral response in channels 4 and 5 of the MSS. The integration of the percentage of incident light over the spectral response of the MSS shows no direct or linear correlation between the chlorophyll concentration and the response of the MSS. However, according to Fig. 2, the maximum of absolute backscattered light is centered in the response of channels 4 and 5.

We might conclude that most energy from the backscattered light from below the surface is due to the plankton organisms and probably affected in the longer wavelength only by a certain degree of chlorophyll. However, this information still can be correlated with biomass or plankton concentrations.

3. QUALITATIVE DIFFERENTIATION BETWEEN SEDIMENTS AND PLANT LIFE

Since sediments in near-coastal areas respond in a way similar to that of chlorophyll within the spectral response of the MSS, it was intended to differentiate in a qualitative study between the effect of sediments suspended in water and chlorophyll on the different channels.

The target for a representative estuary with sediment discharge was the St. John's River in the southern United States. Over cloud-free areas the river discharge showed a higher reflected energy in the visible than the open ocean did. Clouds were very easy to distinguish from sediment-loaded water masses.

The black and white imagery of the channels 0.5-0.6, 0.6-0.7,

0.7-0.8, and 0.8-1.1 μm was color-enhanced to display the reflective properties of seston and chlorophyll concentration (Fig. 3). Channel 4 (0.5-0.6 μm) monitored the effect of chlorophyll as well as sediments and exhibits a diffuse structure in the response of the MSS. The next channel, located at 0.6-0.7 μm, indicates a very pronounced gradient within the sediment plume. This is caused by the position of the second absorption band of chlorophyll at 0.66 μm sediments and the increased absorption of water, which limit the photon penetration depth. The recordings in the near-infrared (0.8-1.1 μm) gave a response only in the near-coastal areas, thus indicating near-surface parameters. The transport of sediments is limited to the coast and is forced toward the south, in agreement with the direction of near-coastal currents and the Coriolis effect.

As a result, we may state that very high concentration of sediments and/or inorganic particulate matter is visible in all four bands of the MSS. Pure phytoplankton populations should cause a response principally in channel 4. This response is the result of increased reflectivity at short wavelengths and the compensation of reflection by absorption in channel 5.

4. TEST SITE DESCRIPTION

Fig. 4 shows a composite of data for the reflected solar

energy between 0.7-1.1 μm as collected by channel 7 of the MSS. The frames were obtained during ERTS-1 overpass of the NW coast of Africa between 32°N and 10°N. The area covered includes Morocco, Spanish Sahara, Mauritania, Senegal, Gambia, Portuguese Guinea, and Guinea. The northern boundary of the test site includes the region of the Anti Atlas mountains in Morocco.

The only important river discharges in the test site are from the Senegal River and the Gambia River. To omit areas with sediment discharge from rivers, ERTS-1 data were interpreted only north of the Senegal River.

5. PLANKTON PATCHINESS AS VIEWED BY ERTS-1

Cape Sim and Cape Ghir

The hydrography along the coast of Morocco was surveyed by Furnestin (1948, 1950, 1959). His temperature maps show that upwelling exists throughout the whole year, with its source at 200 to 400 m. This results in low temperatures and low salinities in the near-coastal region. A typical temperature set for four different seasons is shown in Fig. 5. During wintertime the coastal zone has temperatures below 16.5°C. The southeast/northeast winds develop during the spring with strong horizontal temperature gradients having minimum temperatures around 17°C. Normally the highest upwelling is found during summertime. According to the temperature data, there is evidence that two separated up-

welling areas exist between Cape Ghir and Modagor.

The biological effect of upwelling is demonstrated by the geographic and seasonal distribution of sardines and their eggs. Cape Juby and Cape Ghir show high concentration of biomass (Furnestin and Furnestin, 1959).

One survey made in July, 1972, showed the lowest temperature at 14.5°C. Furnestin (1948) reported data from July and August, 1947, with temperatures not below 16°C for the same area. In accordance with the temperature data, the highest chlorophyll concentration was greater than 3.5 $\mu g.l^{-1}$ and was found in the same location (Fig. 6). Discrete sampling over a period of four weeks smooths out many of the details which may appear in the real distribution of chlorophyll and other surface parameters. Continuous recordings of chlorophyll, temperature and nutrients showed that the distribution of these parameters is much more structured than indicated by the analysis of discrete samples (Fig. 7).

Recordings in the visible with ERTS-1 on September 28, 1972, showed that high plankton concentrations of biomass are inferred by the light gray in the image. The location of the plankton and the discharge of water from the Oued Soness River indicate a very narrow countercurrent in the coastal region. This current was detected by ERTS in September between 29°30'N and 30°15'N. Fig. 9 demonstrates in more detail the color-enhanced near-coastal region, where the river discharge is displayed in purple. The deflection of the river outflow is almost parallel to the coast in the NE direction.

Fig. 10 shows the patchiness of plankton distribution recorded by ERTS-1 on February 20, 1973, close to Cape Sim. The left-hand side shows the recorded energy in the green band as a pictorial display. The position of the frame is shown in the right-hand side of the image composite. In the spectral region between 0.5 and 0.6 μm, the water has the highest photon penetration depth. Therefore, an integrated value for plankton over the penetration of light will be received and no particular structure in the distribution of plankton can be recognized.

The corresponding imagery from the red band of the multispectral scanner is displayed in Fig. 11. Since the photon penetration depth is lower than in the green band, only near-surface phenomena in the water will be observed. The interpretation of this frame showed two cyclonic gyres at Cape Hadid, and one near Cape Sim. With different enhancements of the original negative, more detailed analysis of this current system was achieved. The right-hand side of Fig. 11 shows the near-surface circulation as derived from channel 5.

It must be stressed that this analysis shows only the near-surface features and it is questionable whether these surface currents also reflect the circulation in the deeper layers. Repeated coverage of the area indicated that the direction of surface currents is not permanent. Furnestin (1970) also showed seasonal variations in different planktonic species which indiciates change in intensity of upwelling.

Fig. 12 is an image which was recorded on February 20, 1973, near Cape Ghir. An approach similar to the previous analysis was used to analyze different enhanced imagery material for the current pattern. The derived surface movements of the water masses showed complicated structures in the patterns as detected in the imageries from the northern upwelling region.

Recordings on February 22, 1973, south of Cape Ghir, demonstrated that even in the offshore region, isolated patches in plankton might appear. This is shown in Fig. 13, which depicts primarily oceanic regions at a latitude of about $26^{\circ}30'N$. On March 27, 1973, cloud-free conditions allowed a synoptic view of the upwelling area close to Cape Ghir (Fig. 14). The highest concentration of plankton was detected south of Cape Ghir. The low albedo levels in the near-coastal region again indicated the northward-directed countercurrent. During this time of year, no significant river discharge appears. As a result, we may state that the near-coastal area shows the transport of water masses with low concentration of biomass toward the north.

Since the backscattered light from plankton is most effectively monitored in the green part of the electromagnetic spectrum, the different gray shades in the ERTS-1 imageries over the oceans can be interpreted in terms of plankton concentration. ERTS-1 data showed that two different active upwelling cores with high concentrations of plankton appear between $30^{\circ}N$ and $31^{\circ}N$. Continuous recordings of chlorophyll in the surface water taken prior to the ERTS-1 launch (Fig. 15) confirmed the presence of two well-

developed chlorophyll maxima between Cape Ghir (30°39'N; 09°57'W) and Cape Tefelney (31°05'N; 09°51'W). Historical data reported by Furnestin (1959) also suggest these separated upwelling areas.

Cape Blanc and Cape Timiris

The hydrography between Cape Blanc and Cape Timiris can be described by the T-S diagram based on 16 stations (Allain, 1970) where data were collected between 0 and 800 meters. Two main formations of water masses can be recognized. The first is within the upper 300 meters and can be considered a mixture of surface water and Central South Atlantic water with values of 12°C and 35.35‰ at 300m. The layer between 400 and 800 m consists mainly of Central North Atlantic water with temperatures between 12 and 8°C. The influence of Antarctic Intermediate Water is shown by water with a salinity of 35.05‰ and a temperature of 7°C. Upwelling in this area is limited for water types with temperatures between 18.5° and 20.5°C and salinities between 35.8 and 35.95‰, which show that the upwelling has its origin in the upper 100 meters.

The test site between Cape Blanc and Cape Timiris was repeatedly covered by ERTS. The recordings for August 26, 1974 are shown in Fig. 16 and Fig. 17. Due to the high albedo levels from the Sahara, the white part of the gray level is almost saturated.

Plankton-poor water has low albedo levels which appear black. The oceanic region is partly cloud-contaminated; however, the structure caused by suspended material can be easily recognized. High patchiness in the distribution of plankton as recorded by ERTS was found south of Cape d'Arguin. Isolated patches of plankton had a width of about 1-2 kilometers. A well-pronounced gradient was recognized in the offshore area close to Cape el Sass. A second sharp gradient was found in the same location 30 miles off shore. The comparison between the two recordings in the green and in the red band showed that in the band which recorded the energy between 0.6-0.7 micrometers, plankton is still visible.

The area discussed above was investigated again on November 6, 1972. The red band and the green band are displayed in Fig. 18 and Fig. 19. Cloud contamination appears only in the small portion of the frame south of Cape d'Arguin. A similar patchiness in the distribution of suspended matter was observed but the location of the gradients was different. This indicates that most of the features shown in the frames are not created by the bathymetry. At this period of time, the red channel showed a lower response, which indicates that the concentration of biomass is reduced.

On February 22, 1973, a complete cloud-free image was obtained. The data are displayed in Figs. 20, 21, 22, and 23. The recordings in the red channel and the near-infrared channel (Fig. 23) from the multispectral scanner showed extremely clear conditions

in the atmosphere. The lower gray levels in the Bay de Levrier indicated a low concentration of suspended material. Similar dark areas were observed close to Cape Tafarit. The sharp concentration gradient in the lower-left-hand corner in Figs. 20 and 21 might be a part of the converging high-density water resulting from high evaporation over the Banc d'Arguin. All recordings with the MSS showed that the area east of this convergence is rich in particulate material.

Fig. 24 is a montage of channels 4, 5, 6, and 7 in the Cape Timiris area. It shows the Presquile de Thila, Baile de St. Jean and part of Agnetik. Channels 6 and 7 can be used as cloud discriminators. The recordings of channel 4, therefore, can be used for an estimate of plankton concentration and the location of water boundaries.

Recordings on February 22, 1973, by the NOAA-2 satellite are shown in Fig. 25. The right-hand side of the figure shows the image as obtained by recording the reflectance. The interpretation of the image indicates that cloud-free conditions exist between 15^{o}N and 35^{o}N. An analysis of digitized data showed the distribution patterns for the reflected energy and for the infrared recordings. A sharp gradient visible in the reflection data is caused by the interface between the oceans and the coast line. Cape Blanc can be recognized in the upper-left corner of the digital display. The temperature was not corrected for atmospheric attenuation but patchiness in the temperature distribu-

tion can be used to locate the origin for the place where the coldest water was found. A correction to be added for NOAA-2 data due to atmospheric attention is about four degrees for a blackbody temperature of 290° Kelvin. This would result in a temperature of 21°C in the center of the cold water. The surrounding temperatures are therefore 4-6 degrees higher than the coldest water.

Fig. 26 shows the recordings from June 28, 1973, for channel 5. In agreement with the former observations, high patchiness in the distribution of particulate matter was found. The repeated coverage of the upwelling area between Cape Blanc and Cape Timiris showed the heterogeneity as well as the changes in concentration of plankton in this area. Since coverage was provided only for August, November, February, and June, no estimate about the residence time of the plankton patches can be established. However, from the four observations it is evident that upwelling is present throughout the year and major changes in the concentration of plankton can be observed. The patchiness varies especially with the change of seasons. The southern strong gradient in chlorophyll and/or plankton is connected with the converging water masses from the Banc d'Arguin and was detected during all four seasons. As expected from previous satellite investigations in the infrared region of the electromagnetic spectrum over the Gulf Streams, the northwest coast of Africa and the Somali Current, the gradient undergoes a fluctuation in space and time. This is demonstrated in

Fig. 27, where the position of the plankton gradient is shown for four different seasons. Besides the small-scale fluctuations, it is noticeable that the gradient shifts over only 10 miles (note that the ground resolution of ERTS-1 is about 100 meters).

The distribution pattern of plankton allows a qualitative derivation of the surface movements of the water masses in the investigated area. An example of the interpretation of plankton distribution in terms of surface movements is shown in Fig. 28. From the data obtained in channel 4 and channel 5, the enhancement of separated gray levels allowed a detailed description of the possible transport of plankton in an offshore direction. The main movement of the particle-rich water is toward the boundary. Since no significant horizontal transport of plankton is observed parallel to the boundary, it can be speculated that the plankton is transported in a convergent flow near the boundary. Ship observations for the area are infrequent. Observations made by Dr. Ballester in September, 1972, with continuous recordings, indicated a strong gradient in the temperature and fluorescence with increasing fluorescence toward the coast. The temperature distribution for September 1972 is shown in Fig. 29. It is evident that the strong gradient (see Fig. 27) detected by ERTS-1 is connected with a thermal front caused by upwelling. Fedoseev (1970), using the dynamic topography, discussed the geostrophic circulation of surface waters in the shelf region and concluded that quasi-stationary cyclonic gyres are formed on the eastern boundary of the Canary

Current. The most stationary gyre was observed throughout the year south of Cape Blanc. In light of these observations, the strong gradient detected from space might be the eastern boundary of the cyclonic circulation.

6. QUANTITATIVE EVALUATION OF ERTS-1 DATA FOR AN APPLICATION IN PLANKTON STUDIES

A multi-ship survey in August 1972 showed that maximum gradients of chlorophyll were always found close to the coast, with highest concentration near Cape Juby, as shown in Fig. 30. Since coverage by ERTS-1 was obtained in the Cape Juby region two days after the area was investigated with hydrographical stations and continuous chlorophyll recordings, digitized tapes from channel 4 were computer-displayed.

To derive the position of the coast line with the radiance measurements, we established the frequency histogram of all data. The total picture consisted of 585 lines having 810 samples per line with 47,380 points. An average gray level was 1.14 milliwatts/cm^2/steradian. The frequency histogram for channel 4 is shown in Fig. 31, where all data were normalized to the maximum of 100.

The two maxima in the frequency distribution indicate the different gray levels for water and the adjacent continent. The high radiance of 1.17 to about 1.56 $mw/cm^2/ster.^{-1}$ (i.e., 60 to 80 digital units) corresponds to an albedo of from 0.254 to 0.339

and shows the reflective properties of the desert region. Gray levels between 0.51 and 0.98 mw/cm^2/ster.$^{-1}$ (i.e., 26 to 50 digital units) correspond to albedo levels of 0.110 to 0.213 and can be assigned to the radiance of the ocean.

The frequency distribution shows that gray levels greater than 0.98 m/cm^{-2}/ster.$^{-1}$ (albedo equals 0.213) are caused by the coastal features of the continent. Consequently, a threshold level was developed for the position of the waterline to be indicated by radiances less than 0.98 mx/cm^{-2}/ster.$^{-1}$.

Fig. 32 shows a computer printout where characters were assigned to the radiance. Only every 12th line was used, with a sample spacing of 12. The gradient visible by the assigned character 0 shows the position of the coast line. The region near Cape Juby shows high radiance caused by plankton. The transport of plankton within the coastal current can be seen by the symbols 1 and 8 . Radiance less than 0.61 mw/cm^{-2}/ster.$^{-1}$ had no assigned symbol. Therefore, the offshore area in the northwest corner of the display indicated with low radiance shows low concentration of plankton organisms.

Fig. 33 gives the analysis of radiation data as obtained from the generated grid print map over an area of 30 km. The isolines of radiances were smoothed over about eight grid points. The position of the coast line was established by the maximum gradient at the interface between the continent and the ocean. The isoline closest to the coast was three grid print points.

Oceanic regions with high productivity have a thin eutrophic layer; consequently, the photon penetration depth is very shallow. Readings with the Secchi disc in the upwelling area near Cape Juby showed only five meters, as a result of the light attenuation of plants. Highest radiance can be found in the near-coastal waters where upwelling is expected to be strongest.

Continuous recordings of chlorophyll concentrations during the ground truth program in the upwelling area along the NW coast of Africa showed patterns similar to those derived with ERTS-1. (Fig. 34 The recordings taken parallel to the coast showed variations in the chlorophyll concentration having the same spacing as the ERTS-1 observations. From these measurements we can conclude that the patchiness seen in the image in Fig. 34 is caused by biomass, and not by sediments or inorganic particulate material.

An evaluation using the gray scale on the image display of ERTS data for an estimate of biomass was done for oceanic region without river discharge.* The comparison between the gray scale on the channel 4 imageries and the mean biomass concentration is shown in Fig. 35. Values were selected from areas where dominantly natural plankton populations were expected. Although the displayed data give only a rough estimate, we can conclude that the biomass in oceanic regions can be characterized semi-quantitatively by using the grayscale in the original black and white imageries. Each gray step in the scale corresponds to about 20 $\mu g \cdot l^{-1}$. This means that water masses with small differences in chlorophyll con-

*The biomass was estimated by using the average chlorophyll concentration of 2.5% in diatoms.

centration can be recognized in the imageries.

To understand the significance of remotely sensed sea surface chlorophyll or biomass measurements, the validity of surface chlorophyll measurement for the total biomass within the euphotic zone was established.

The raw data used in this approach were collected by the German R.V. "Alexander von Humbolt" from 1 July, 1970 to 23 November, 1970. The data were published by Schemainda, Schulz, and Nehring (1971). Data were recorded at depths of 1, 5, 10, 15, and 20 meters. Values of chlorophyll concentration and ^{14}C uptake were integrated over twenty meters and the base 10 log of these values was used. Correlations were made between the surface chlorophyll concentration and the integrated chlorophyll concentration over 20 meters (Fig. 36), the surface chlorophyll concentration and the surface ^{14}C uptake rate, the surface ^{14}C uptake rate and the integrated productivity. Lorenzen, in 1970, made similar correlations between 1) surface chlorophyll and primary productivity and 2) surface chlorophyll and total chlorophyll. The data used, however, "include those that might reasonably be expected anywhere in the oceans" and so are not oriented to a specific area, as the data in this paper are. Below is a comparison of data used in both studies.

A distinction should be noted concerning the values used for the euphotic zone. Lorenzen used the 1% incident radiation as the bottom of the euphotic zone; his range of values was 10-91

meters. Since 1% light levels were not available in the data being presented, the depth of 20 meters throughout was taken as the best estimate possible.

In 1964, Guillén, Mendiola, and Rondan published a correlation between primary productivity at 0 meters and primary productivity of the water column (Costlow, 1971). The data was collected in an upwelling area on the west coast of South America between 4^{o} and 12^{o} S latitude. Comparison between this data and the Lorenzen data is made in Table 1.

Neither the actual data points nor the correlation coefficients are given in the Lorenzen or Guillén et al. studies. Therefore, except for the r and r^2 values (representing the fraction of the total sum or sums of squares that can be attributed to the regression line) and the graphs presented, it is difficult to say how well these previous studies agree with this paper's correlations. All the correlations seem significant; for example, an accurate prediction should be able to be made about primary productivity of the euphotic zone from knowledge of one parameter, such as chlorophyll concentrations, and a defined relationship (equation) for the area being studied.

7. CONCLUSION

From the analyzed ERTS-1 data we derive the following conclusion:

1. According to the spectral properties of light backscattered from natural plankton populations, mainly channel 4 (0.5-0.6 µm) and channel 5 (0.6-0.7 µm) can be used to detect plankton. It was found that chlorophyll has only a minor effect on the signals obtained from plankton blooms. This is indicated by the fact that the intensity of backscattered light is proportional to the concentration of plankton in channel 4.

2. The ERTS-1 recordings showed the complex pattern in plankton distribution as they could never be resolved with multiship operations. Repeated coverage within three months showed drastic changes. With the coverage obtained over the test site it was not possible to determine the residence time or response time of plankton growth to hydrographic influences. We estimate that the changes in patterns of plankton population might be so fast that they cannot be resolved within the time frame of ERTS-1. It might be necessary to have daily coverage or even repeated coverage within one day.

3. The location and shape of the plankton blooms can be used to derive current patterns which can hardly be detected aboard ships. One example was the very narrow countercurrent in the near-coastal region in the vicinity of Cape Ghir.

The gray scale in the imageries of channel 4 can be used to estimate semi-quantitatively the amount of biomass in the water.

It was estimated that one gray step corresponds to about 20 µg biomass per liter.

A. Surface Chlorophyll

Lorenzen	0.04-28.00 µg/l
Our Study	1.60-14.70 µg/l

B. Integrated Euphotic Zone Primary Productivity

Lorenzen	0.06-11.00 $g^{14}C/m^2 \cdot d$	Euphotic Zone = $\sum_{10-91m}^{0m}$
Our Study	1165.1-9272.8 $\mu g^{14}C/m^2 \cdot d$	Euphotic Zone = $\sum_{20m}^{1m}$
Guillén et al.	0.18-0.61 $g^{14}C/m^2 \cdot d$	Water Column

C. Integrated Euphotic Zone Chlorophyll

Lorenzen	7.0-277.0 mg/m^2
Our Study	355-3140 $\mu g/m^2$

D. *Primary Production at 0 or 1 meter*

Guillén et al.	5-93 $mg^{14}C/m^3 \cdot d$
Our Study	12.1-104.5 $\mu g^{14}C/l \cdot d$

TABLE 1: Data range for correlation between primary productivity data

	equation	r^2	r
Lorenzen*	$\log \sum_{10-91m}^{0m} Chl = .620 \log \text{surface Chl} + 1.514$	.817	.904
Our Study	$\log \sum_{20m}^{1m} Chl = .877 \log 1m\ Chl + 2.364$	.432	1.398
Lorenzen	log primary productivity = .475. log surface Chl + .185	.539	.734
Our Study	log primary productivity (1m) = .715 log Chl(1m) + 1.054	.6575	.029
Our Study	$\log \text{primary productivity} \sum_{20m}^{1m} = .684 \cdot \log Chl \sum_{20m}^{1m} + 1.444$	.666	-.001
Guillén et al.	primary productivity of water column =0.2062 + 0.0043 primary prod.(0m)		0.87
Our Study	$\log \sum_{20m}^{1m} \text{primary productivity} = .931 \cdot \log \text{primary prod. at 1m} + 2.078$	.199	.002

*The data published by Lorenzen used natural log arithmetic values. Conversion to log base 10 was made for this comparison.

TABLE 2: Statistical evaluation of correlation between primary productivity data.

8. ABBREVIATIONS USED

EMR	Electromagnetic Radiation
ERTS	Earth Resources Technology Satellite
ETS	Electron Transport System
GSFS	Goddard Space Flight Center
IDCS	Image Dissector Camera System
ITC	Intertropical Convergence
MRIR	Medium Resolution Infrared Radiometer
MSS	Multispectral Scanner
NASA	National Aeronautics and Space Administration
NESS	National Environmental Satellite Survey
NOAA	National Oceanic and Atmospheric Administration
THIR	Temperature Humidity Infrared Radiometer

9. FIGURE CAPTIONS

Fig. 1: Wavelength dependent radiance caused by particulate and dissolved matter. For explanation see text.

Fig. 2: Spectral response in channel 4 and 5 of the MSS on ERTS-1 and backscattered light over oceanic regions with different chlorophyll concentrations.

Fig. 3: Color enhancements of channel 4, 5, 6 and 7 from ERTS-1 recordings.

Fig. 4: Composit of data obtained by ERTS-1 in channel 7.

Fig. 5: Seasonal distribution in temperature, reconstructed from data reported by Furnestin (1959).

Fig. 6: Chlorophyll distribution in July 1972 in the Cape Ghir region.

Fig. 7: Continuous recordings of nitrate, temperature and chlorophyll in a perpendicular section to Cape Ghir.

Fig. 8: Recorded energy in ERTS-1 band 4 (0.5 to 0.6 μm) on September 28, 1972.

Fig. 9: Color enhanced and original ERTS-1 image showing the northward transportation of particulate material.

Fig. 10: ERTS recordings on 20 February 1973 in the Cape Sim area, channel 4.

Fig. 11: ERTS recordings on 20 February 1973 in the Cape Sim region, channel 5.

Fig. 12: ERTS recordings on 20 February 1973 in the Cape Ghir region in channel 4.

Fig. 13: ERTS recordings in channel 4 on 22 February 1973 at about 26°30'N (center of the image).

Fig. 14: ERTS recordings in channel 4 on 27 March 1973 in the Cape Ghir region.

Fig. 15: Continuous chlorophyll recordings between Cape Ghir (left) and Cape Tefelney (right) in July 1972.

Fig. 16: Recorded energy in band 4 (0.5 to 0.6 µm) on August 26, 1972. Center coordinates of the image are 20°05'N, 16°16'W.

Fig. 17: Recorded energy in band 5 (0.6 to 0.7 µm) on August 26, 1972. Center coordinates of the image are 20°05'N, 16°16'W.

Fig. 18: Recorded energy in band 5 (0.6 to 0.7 µm) on November 6, 1972. Center coordinates of the image are 20°05'N, 16°16'W.

Fig. 19: Recorded energy in band 4 (0.5 to 0.6 µm) on November 6, 1972. Center coordinates of the image are 20°05'N, 16°16'W.

Fig. 20: Recorded energy in band 4 (0.5 to 0.6 µm) on February 22, 1973. Center coordinates of the image are 20°16'N, 16°19'W.

Fig. 21 Recorded energy in band 5 (0.6 to 0.7µm) on February 22, 1973. Center coordinates of the image are 20°16'N, 16°19'W.

Fig. 22: Recorded energy in band 6 (0.7 to 0.8 μm) on February 22, 1973. Center coordinates of the image are $20^{\circ}16'N$, $16^{\circ}19'W$.

Fig. 23: Recorded energy in band 7 (0.8 to 1.1 μm) on February 22, 1973. Center coordinates of the image are $20^{\circ}16'N$, $16^{\circ}19'W$.

Fig. 24: ERTS-1 coverage in the Cape Timeris region on February 22, 1973.

Fig. 25: Recordings with the NOAA-2 satellite on February 22, 1973. The shaded areas show reflectance values higher than 20 (arbitrary units) and temperatures below $288^{\circ}K$ (uncorrected infrared data).

Fig. 26: Recorded energy in band 5 (0.6 to 0.7 μm) on June 28, 1973. Center coordinates of the image are $28^{\circ}17'N$, $16^{\circ}19'W$.

Fig. 27: Seasonal variation in the plankton gradient south of Cape Blanc. Data analysis is based on recordings by ERTS-1 using the highest gradients of albedo in channel 4.

Fig. 28: Derived plankton patterns from ERTS-1 coverage and their pathway.

Fig. 29: Temperature distribution between Cape Blanc and Cape Timeris.

Fig. 30: Chlorophyll distribution along the NW Coast of Africa based on discrete surface sampling during August 1972.

Fig. 31: Frequency histogram for channel 4 near Cape Juby.

Fig. 32: Computerized data from the Cape Juby region shown in Fig. For explanation see text.

Fig. 33: Radiation map as obtained from ERTS-1 recordings in channel 4 over Cape Juby.

Fig. 34: Continuous chlorophyll recordings based on fluorescence measurements and color ratios built from ERTS-1 data.

Fig. 35: Comparison between the grey scale and averaged biomass concentration over a depth of 30m. Each step of the grey scale has one arbitrary unit starting with 1 at the dark end of the scale.

Fig. 36: Statistical comparison between surface chlorophyll measurements and the total integrated concentration of chlorophyll within the euphotic zone.

10. ACKNOWLEDGEMENTS

This research was sponsored by NASA under Contract No. NAS5-21784.

I would like to acknowledge the help of many of my colleagues who contributed to the program. Within the CINECA program, space on research vessels was made available to collect ground truth data through Dr. A. Thiriot, France, and Dr. G. Cabrera, Spain. Data exchange was initiated with Dr. K.F. Bowden, England, and Dr. W. Nehring, German Democratic Republic. Dr. A. Strong provided the digitized data in Fig. 25. Data used for the graph in Fig. 1 were recorded by Dr. W. Hovis, GSFC.

Dr. R. Curran, NASA Goddard Space Flight Center, contributed significantly with his research and discussions. Technical help must be acknowledged to Mrs. E. Ganzman, J. Schaefer, M. Maerker, M. Tabor, and D. Jay at the College of Marine Studies, University of Delaware.

The NASA Scientific Monitor for this program was Mr. J. Greave, NASA Goddard Space Flight Center, Greenbelt, Md.

Editorial assistance for the final draft was provided by Ms. J. Piorko.

The correlations given in Tables 1-2 and Fig. 36 were computed by P.S. Tabor.

REFERENCES

Allain (1970). Les Conditions hydrologiques sur la bordure atlantique de l'Afrique du Nord'Ouest. Cons. Int. Explor. Mer, Rapp. Proc. Verb. 159, 25-29.

Clarke, G.L., G.C. Ewing and C.L. Lorenzen (1970). Spectra of backscattered light from the sea obtained from aircraft as a measure of chlorophyll concentration. Science 20, 1119-1121.

Curran, R.J. (1972). Ocean color determination through a scattering atmosphere. Applied Optics 11, 1857-1866.

Fedoseev, A. (1970). Geostrophic circulation of surface waters on the shelf of north-west Africa. Rapp. Proc. Verb. Cons. Int. Expl. Mer. 159: 32-37.

Furnestin, J. (1948). L'Hydrologie cotière du Maroc. Com. Oceanogr. Et Côtes, Maroc. Bulletin Scientifique 4, 7-28.

_____. (1950). Hydrologie cotière du Maroc et du detroit canarien. Comité océanographique et d'études de Côte du Maroc, 6. 19-60.

_____. (1959). Hydrologie du Maroc Atlantique. Rev. Trav. Inst. Peches. marit. 23, 7-77.

Furnestin, J. and M.-L. Furnestin (1959). La reproduction de la sardine et de l'anchois des cotes atlantiques du Maroc. Revue Trav. Inst. (scient. tech) Pech. marit. 23, 79-104.

Furnestin, M.-L. (1970). Rapport sur le plankton. Cons. Int. Explor. Mer, Rapp. Proc. Verb. 159, 90-115.

Guillen, O., B.R. de Mendiola, and R.I. de Rondan. (1964). In Fertility of the Sea, Vol. 1 (D.C. Costlow, ed.).

Lorenzen, C.J., Limnology and Oceanography, Vol. 15, No. 3, (May, 1970). 479-480.

Schemainda, R., S. Schulz, and D. Nehring, International Council for Exploration of the Sea; Hydrography Comm., C.M. 1971/C:9.

_____. (1972). Geod. Geoph. Veroff. R IV H.7. Teil I.

Yentsch, C.S., (1960). The influence of phytoplankton pigments on the color of sea water. Deep-Sea Res. 7, 1-9.

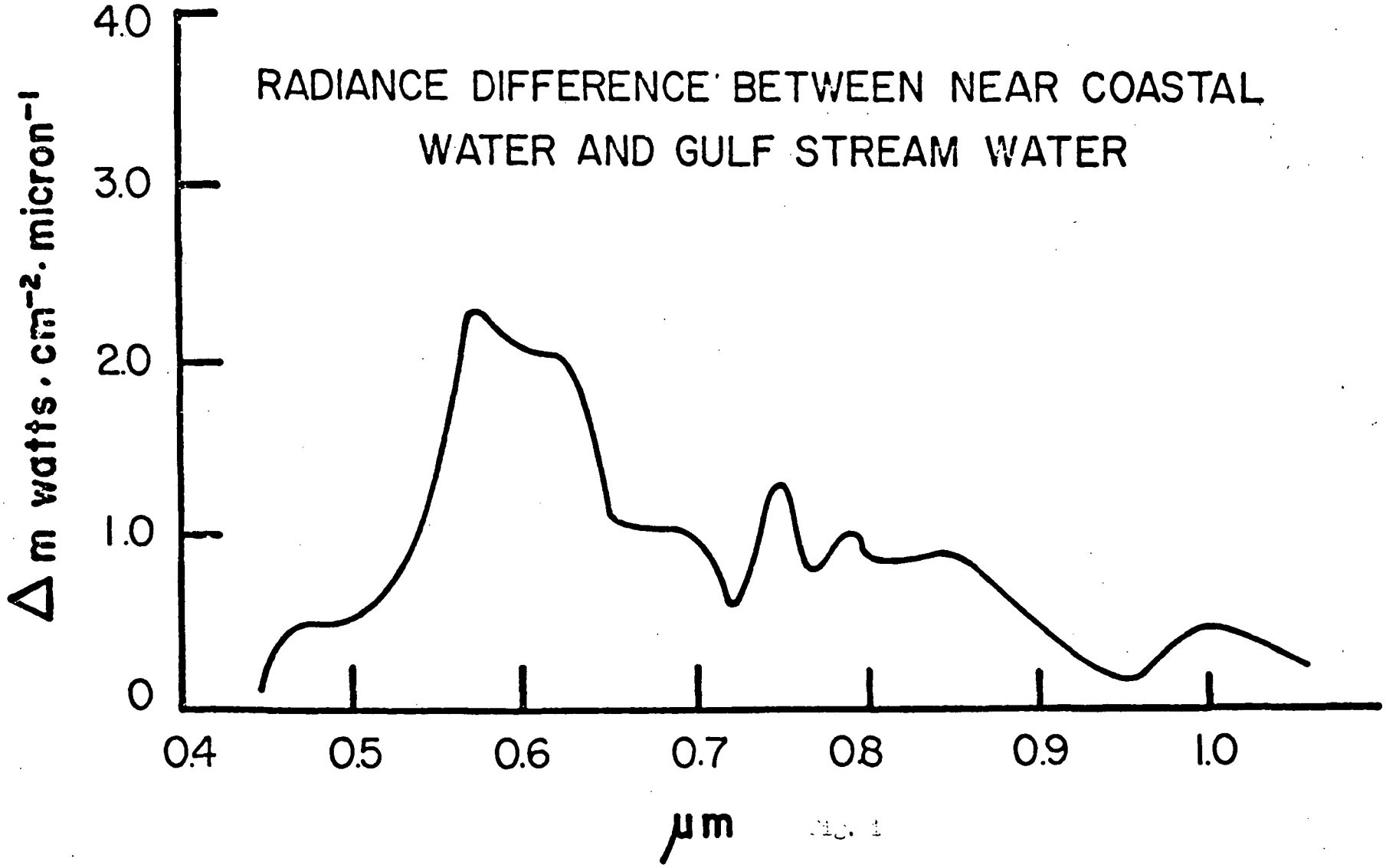
RADIANCE DIFFERENCE BETWEEN NEAR COASTAL WATER AND GULF STREAM WATER
Δ m watts · cm⁻² · micron⁻¹
4.0
3.0
2.0
1.0
0
0.4
0.5
0.6
0.7
0.8
0.9
1.0
μm

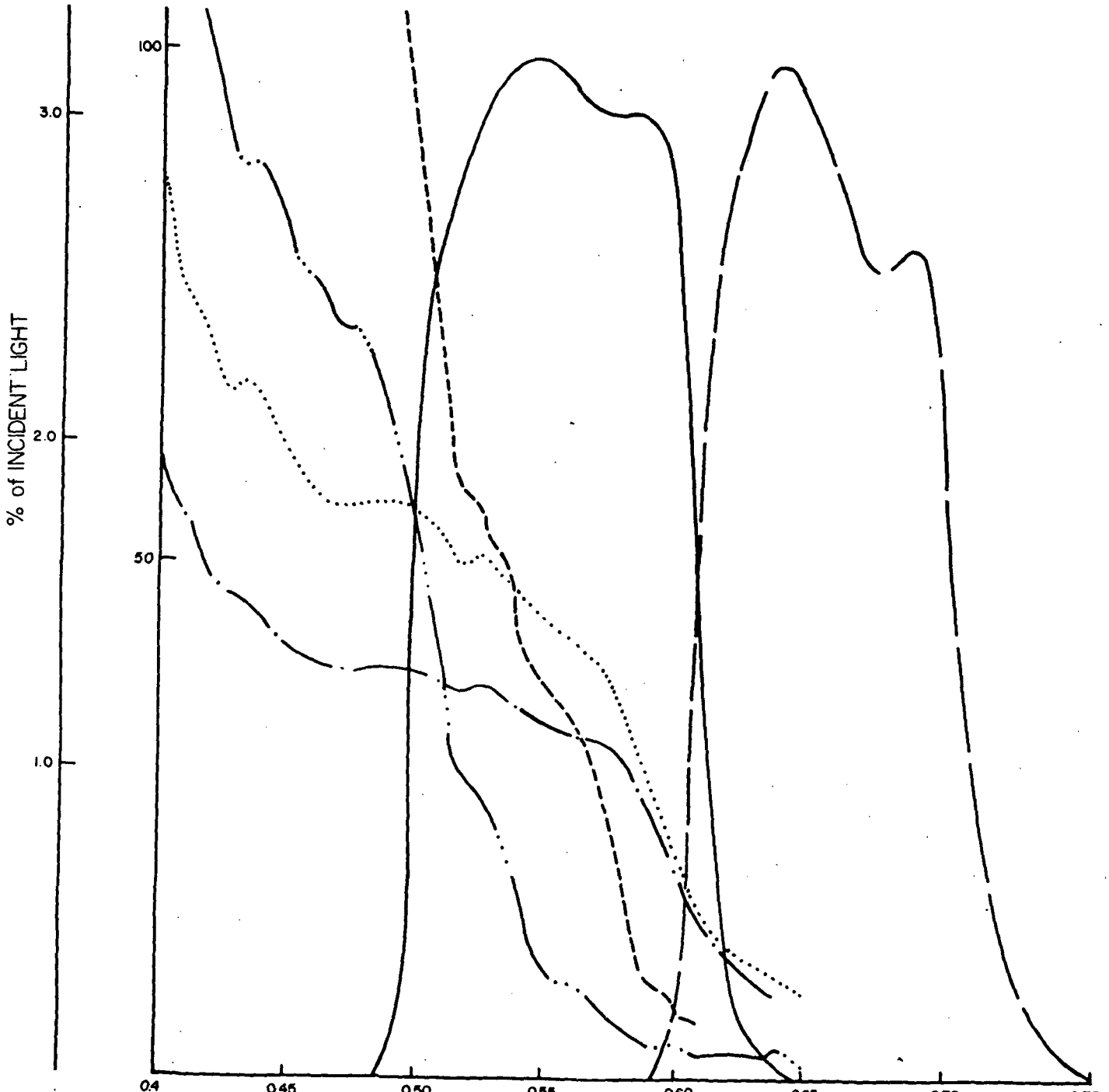

Fig. 2

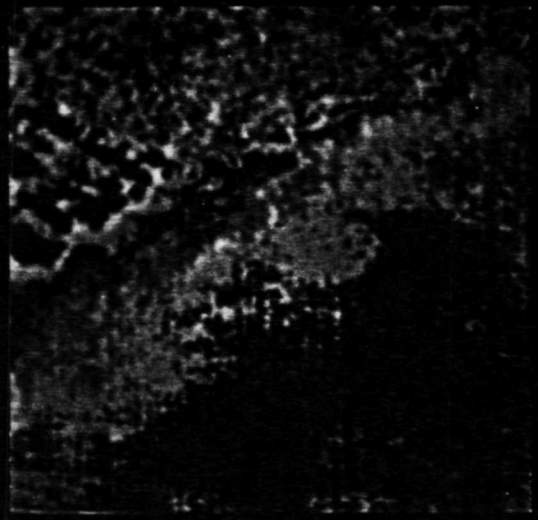

0.5–0.6 μm

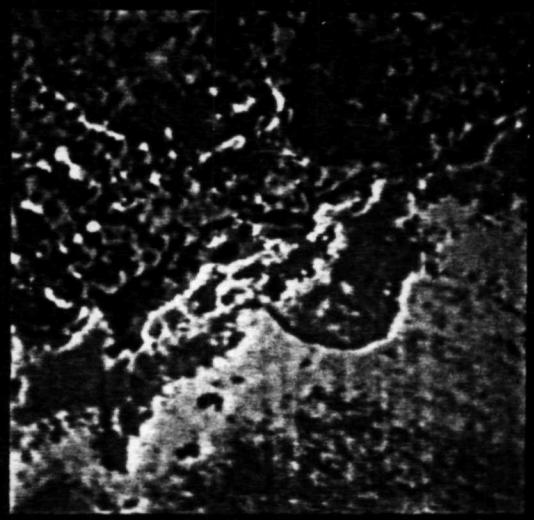

0.6–0.7 μm

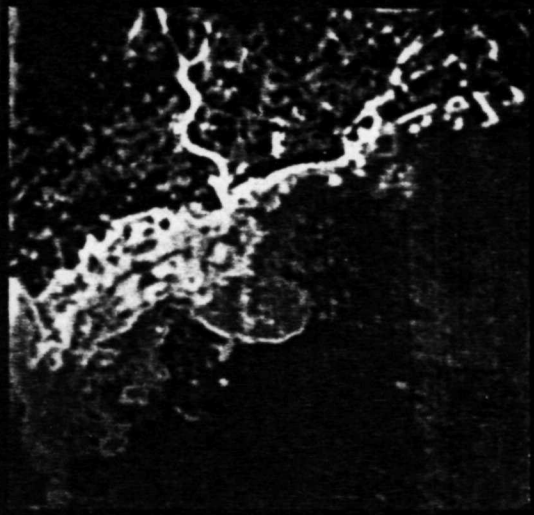

0.7–0.8 μm

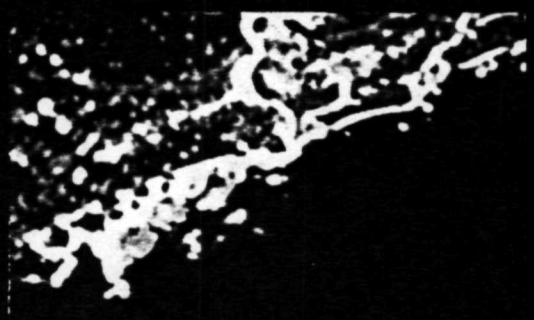

0.8–1.1 μm

ST. JOHN'S RIVER ESTUARY

Fig. 3

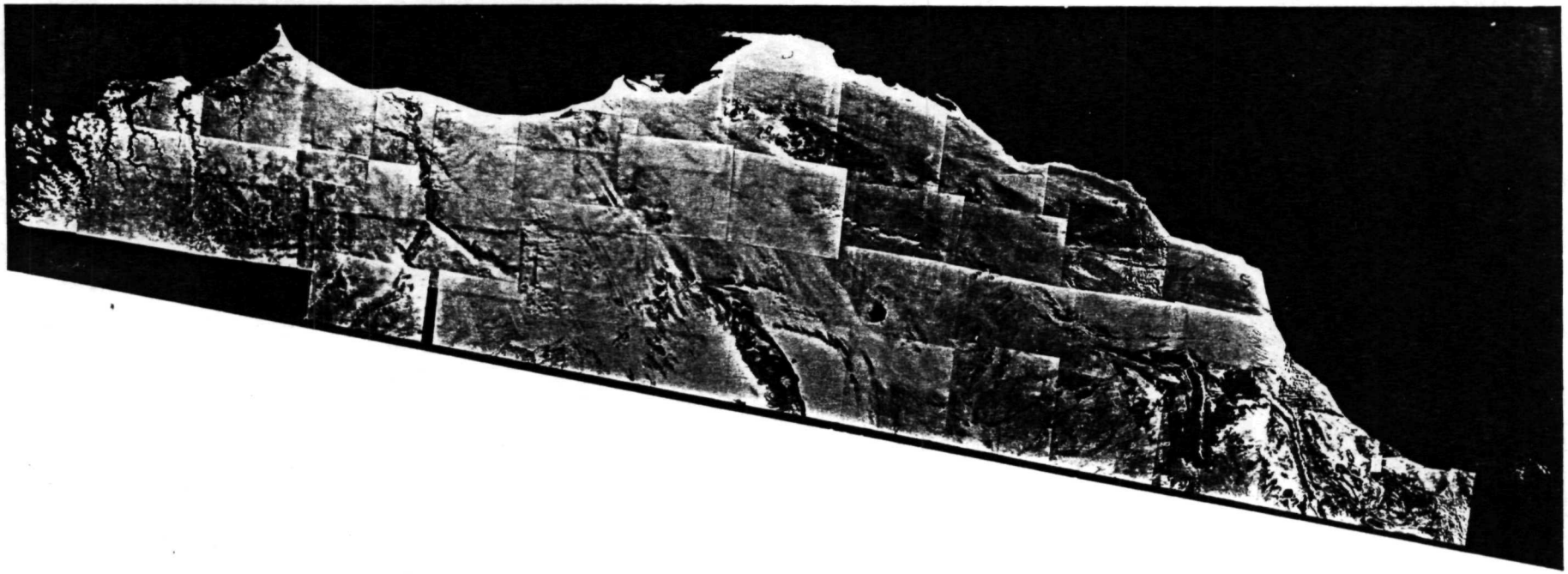

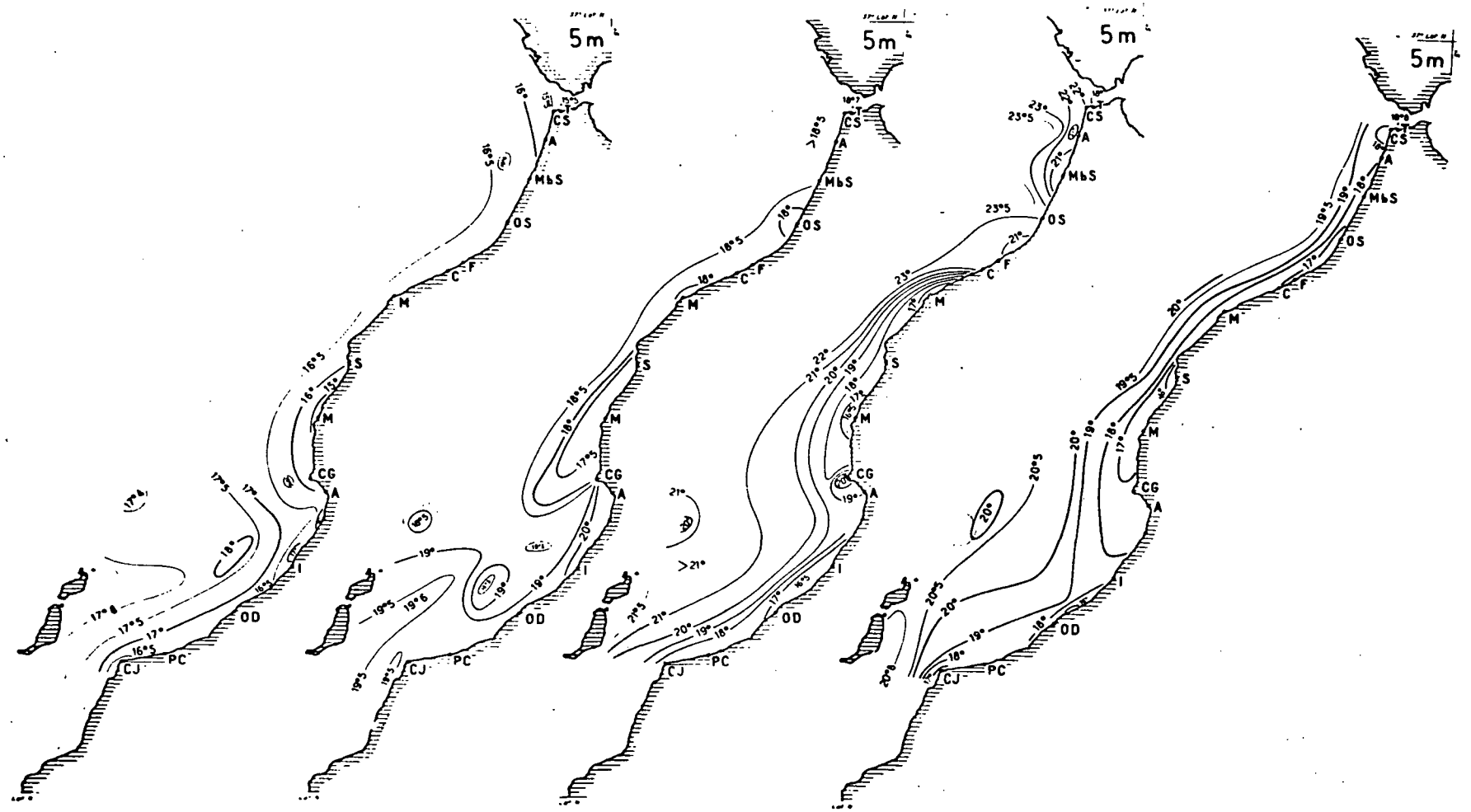

Fig. 5

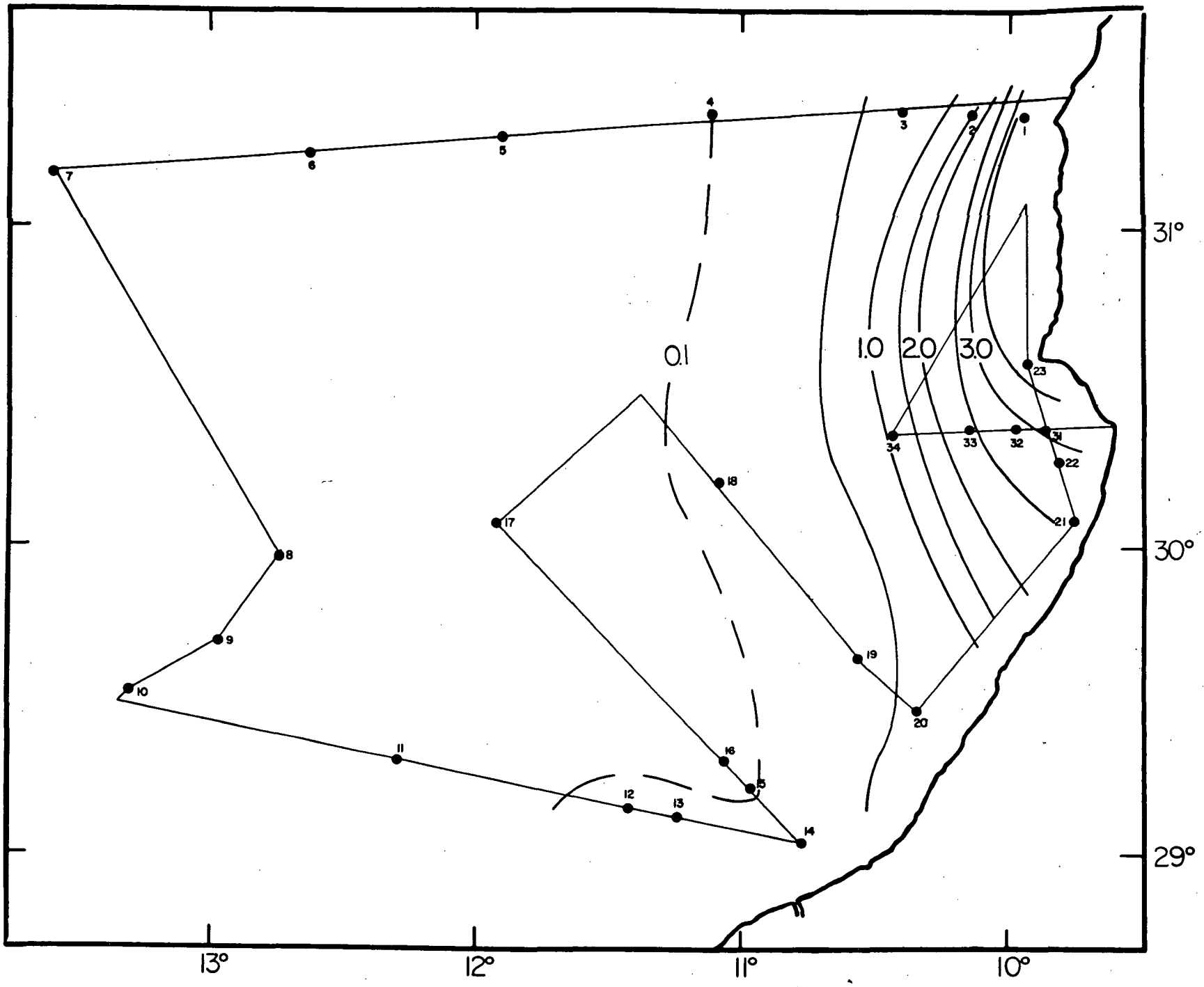
0.1
1.0
2.0
3.0
31°
30°
29°
13°
12°
11°
10°

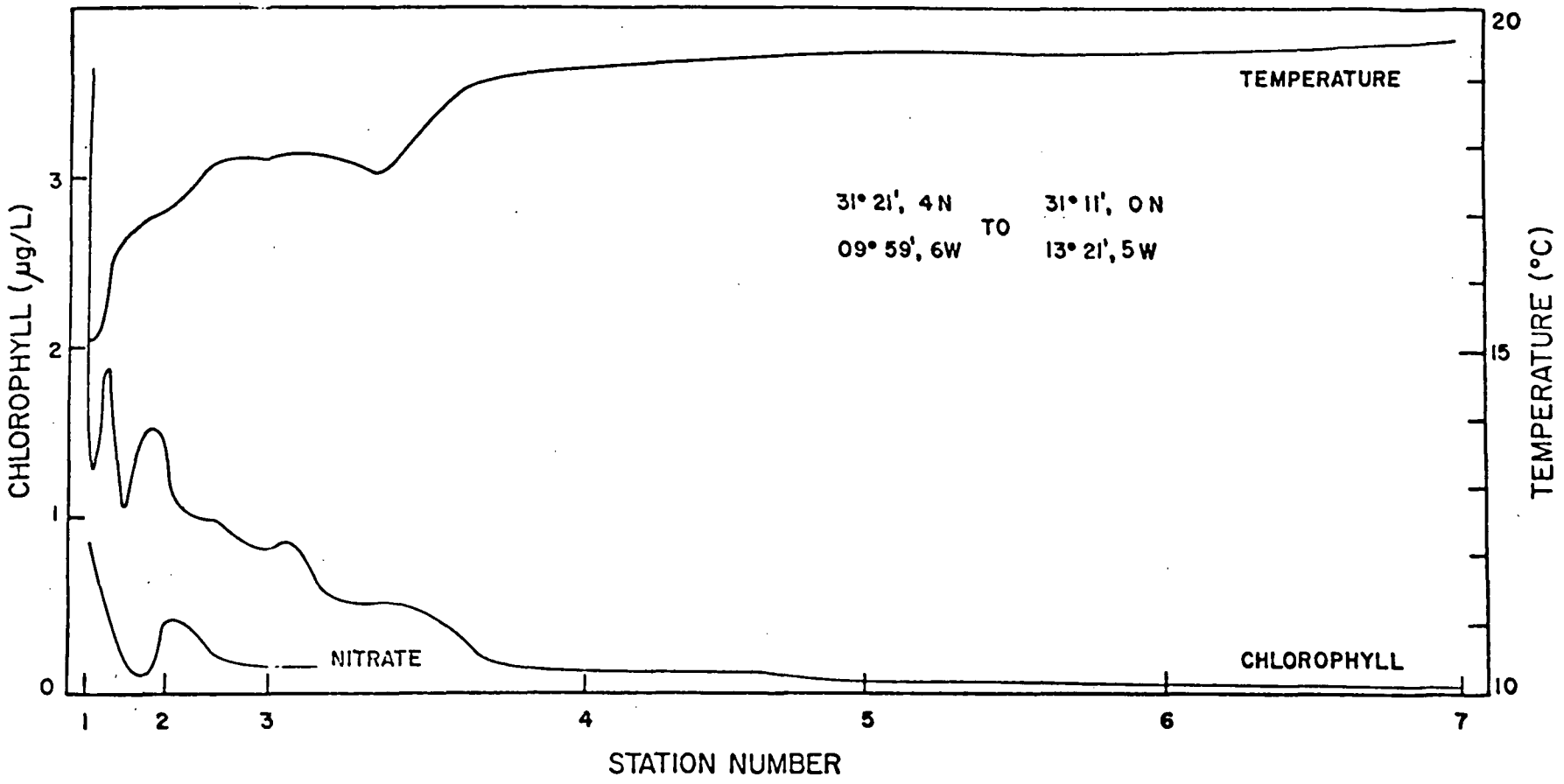
TEMPERATURE
31° 21', 4 N
09° 59', 6W
TO
31° 11', 0 N
13° 21', 5 W
NITRATE
CHLOROPHYLL
CHLOROPHYLL (µg/L)
TEMPERATURE (°C)
STATION NUMBER
0
1
2
3
10
15
20
1
2
3
4
5
6
7

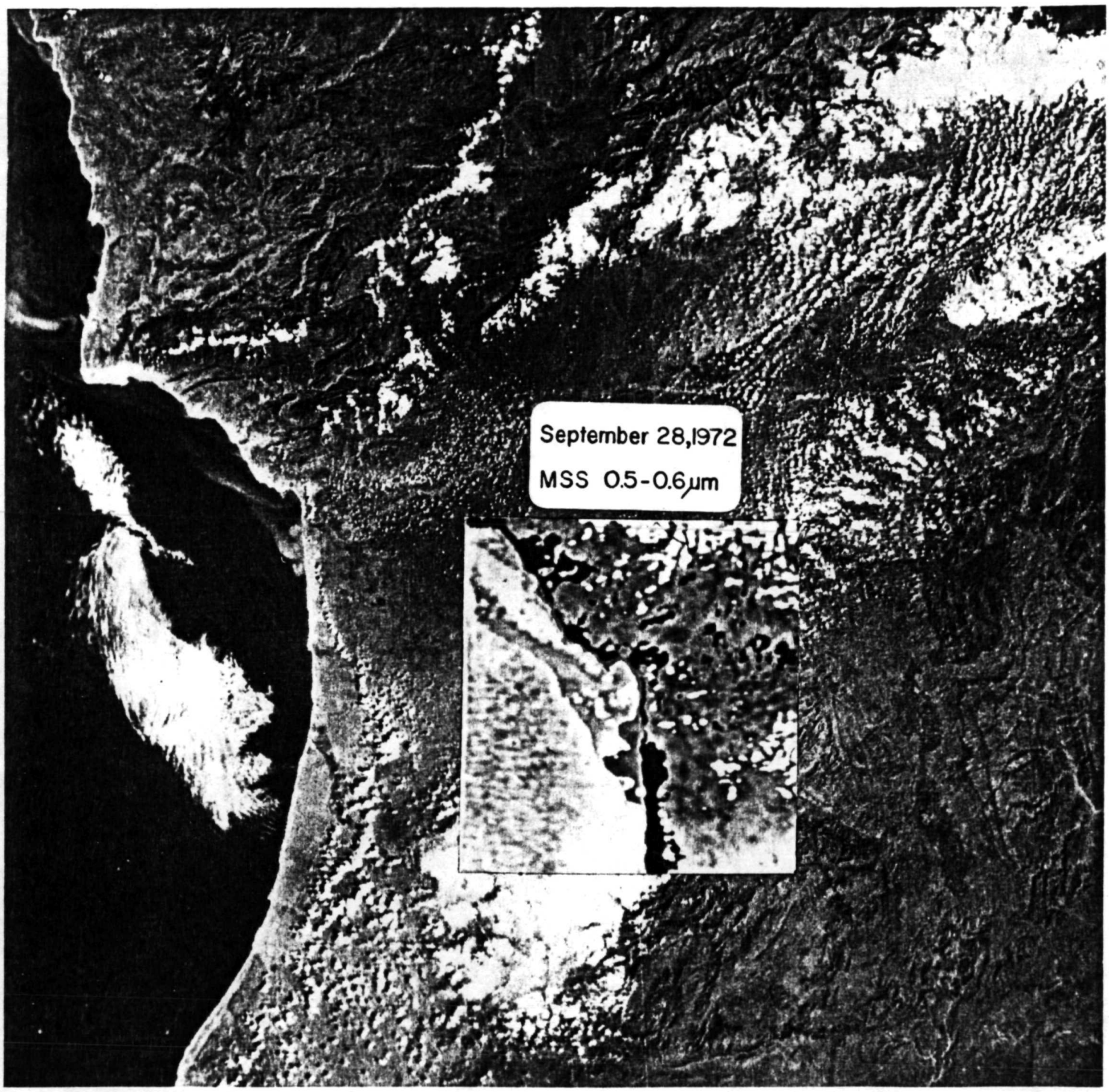
September 28,1972
MSS 0.5-0.6μm

UPWELLING & PLANKTON PATTERNS
NORTH-WEST AFRICA

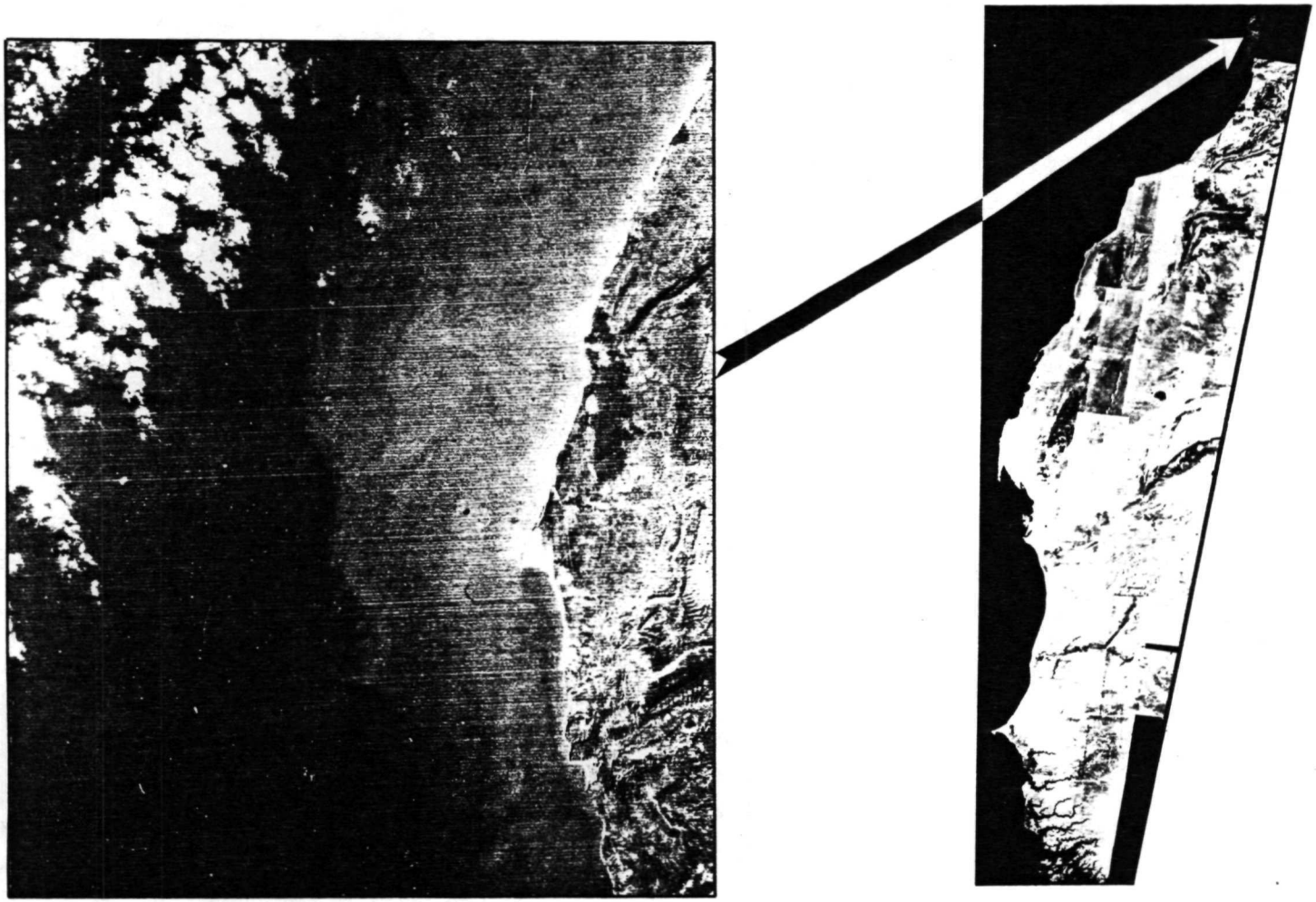

ERTS-1 (GREEN BAND) 20 FEBRUARY 1973

NASA G-74-04779

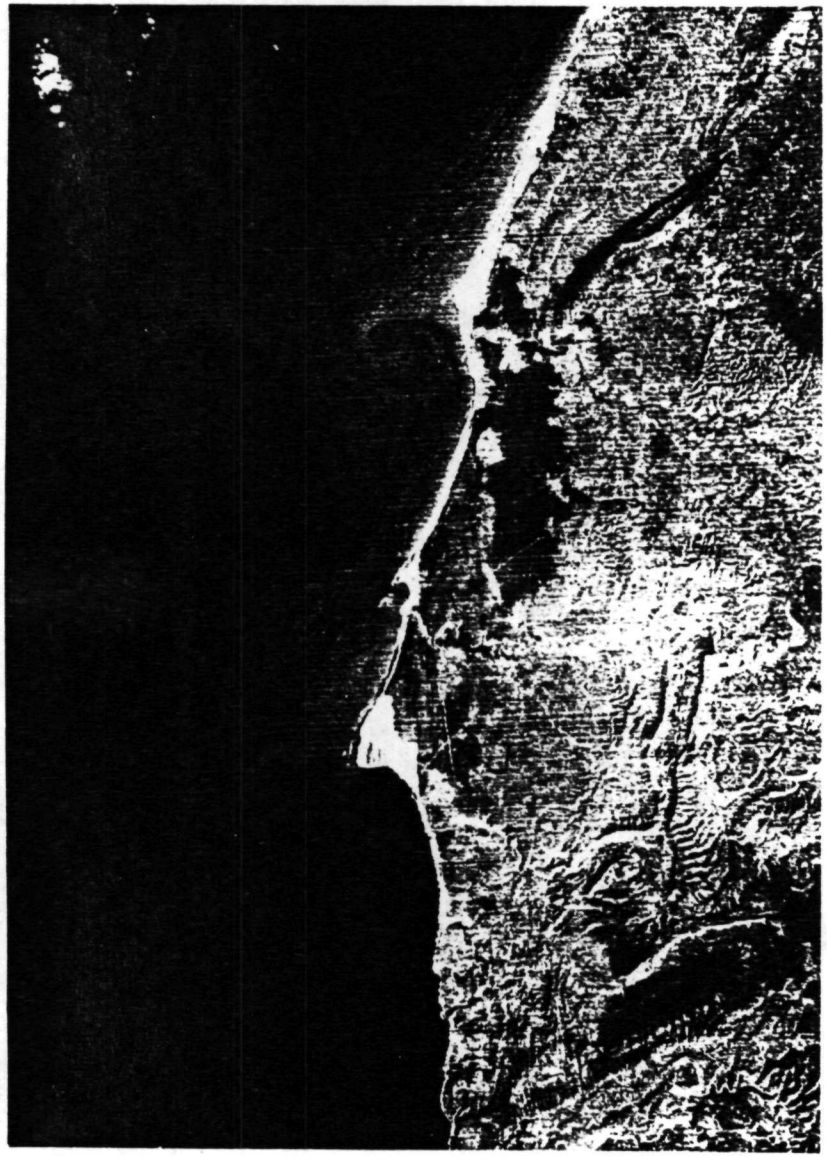

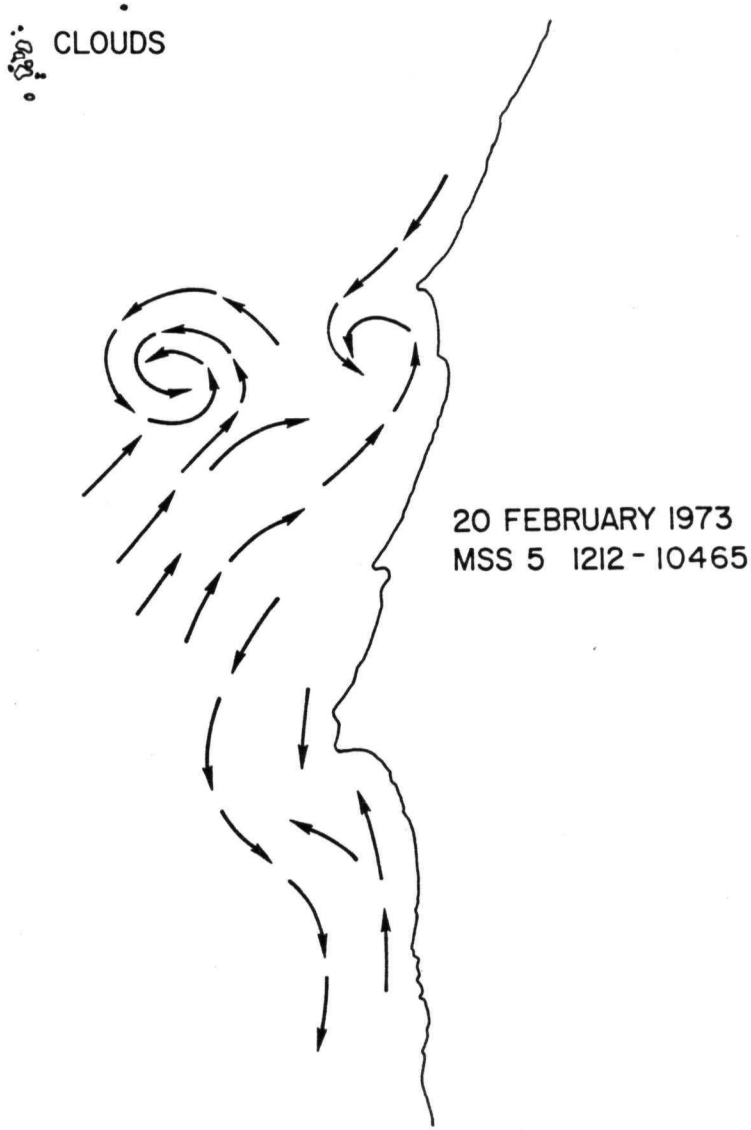
CLOUDS
20 FEBRUARY 1973
MSS 5 1212 - 10465

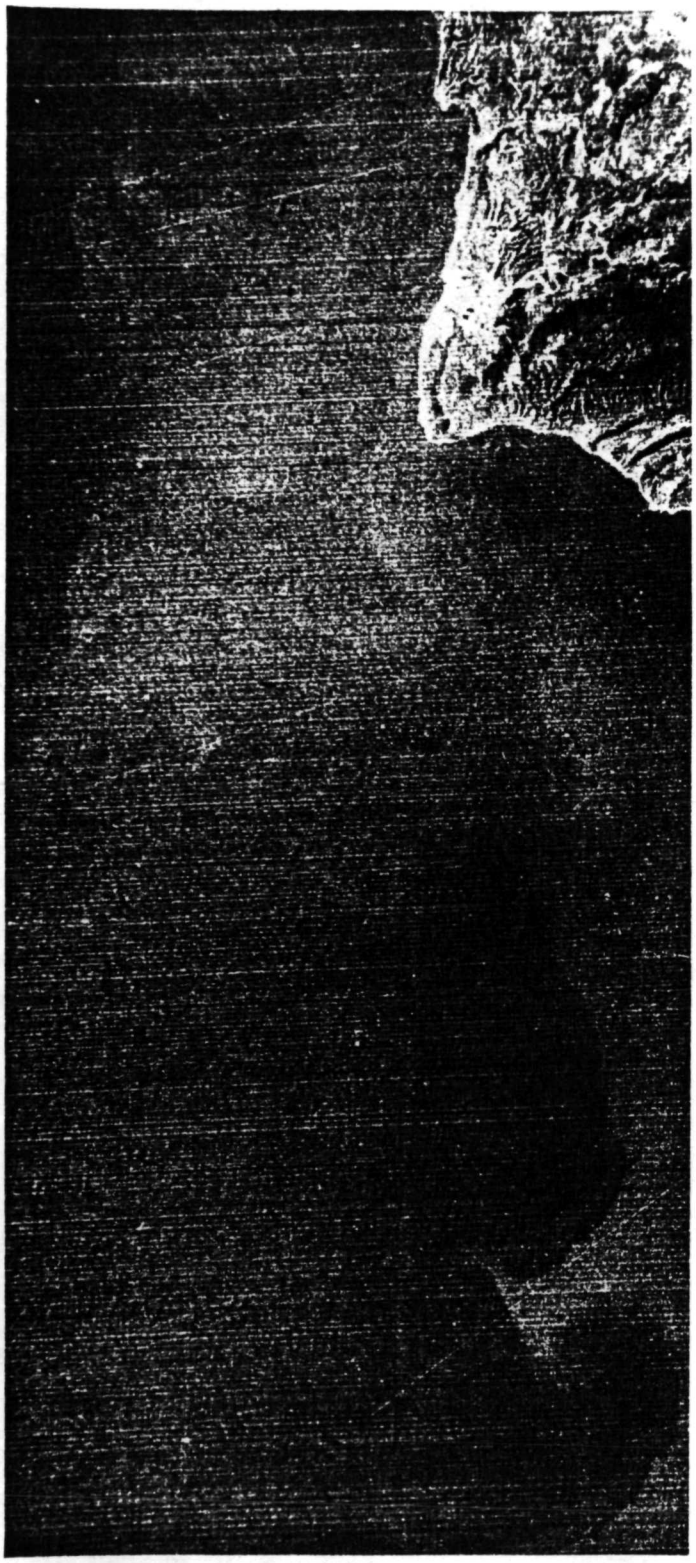

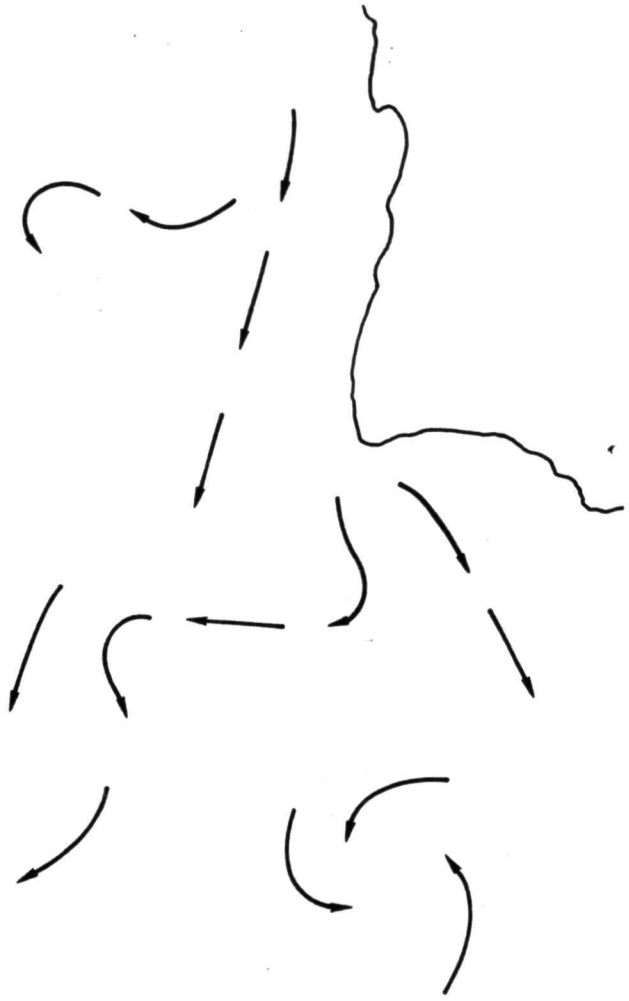

20 FEBRUARY 1973
MSS 4 1212-10471

Fig. 12

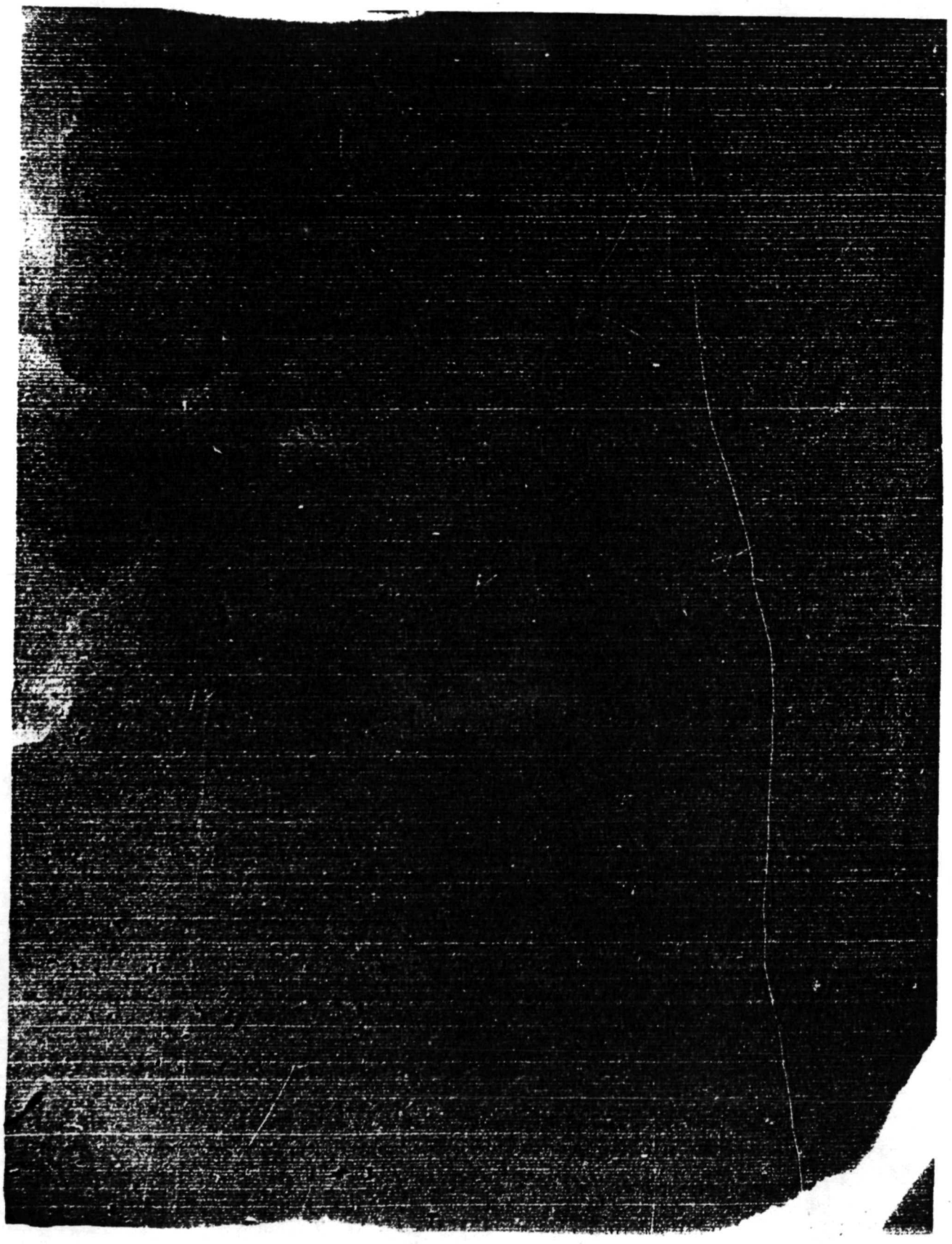

Fig. 1

UPWELLING & PLANKTON PATTERNS
NORTH-WEST AFRICA

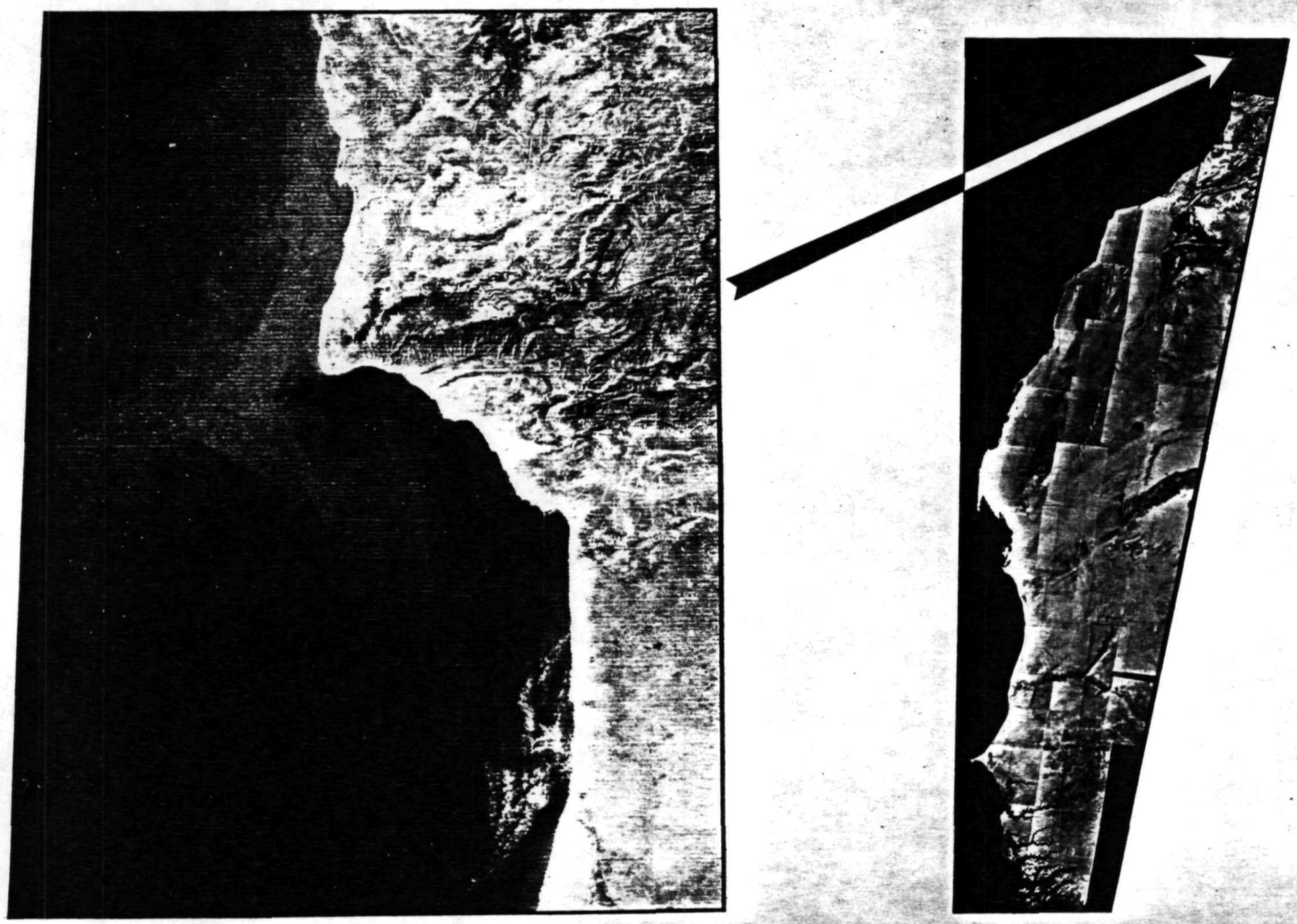

ERTS-1 (GREEN BAND) 27 MARCH 1973

Fig. 14

NASA G-74-C4780

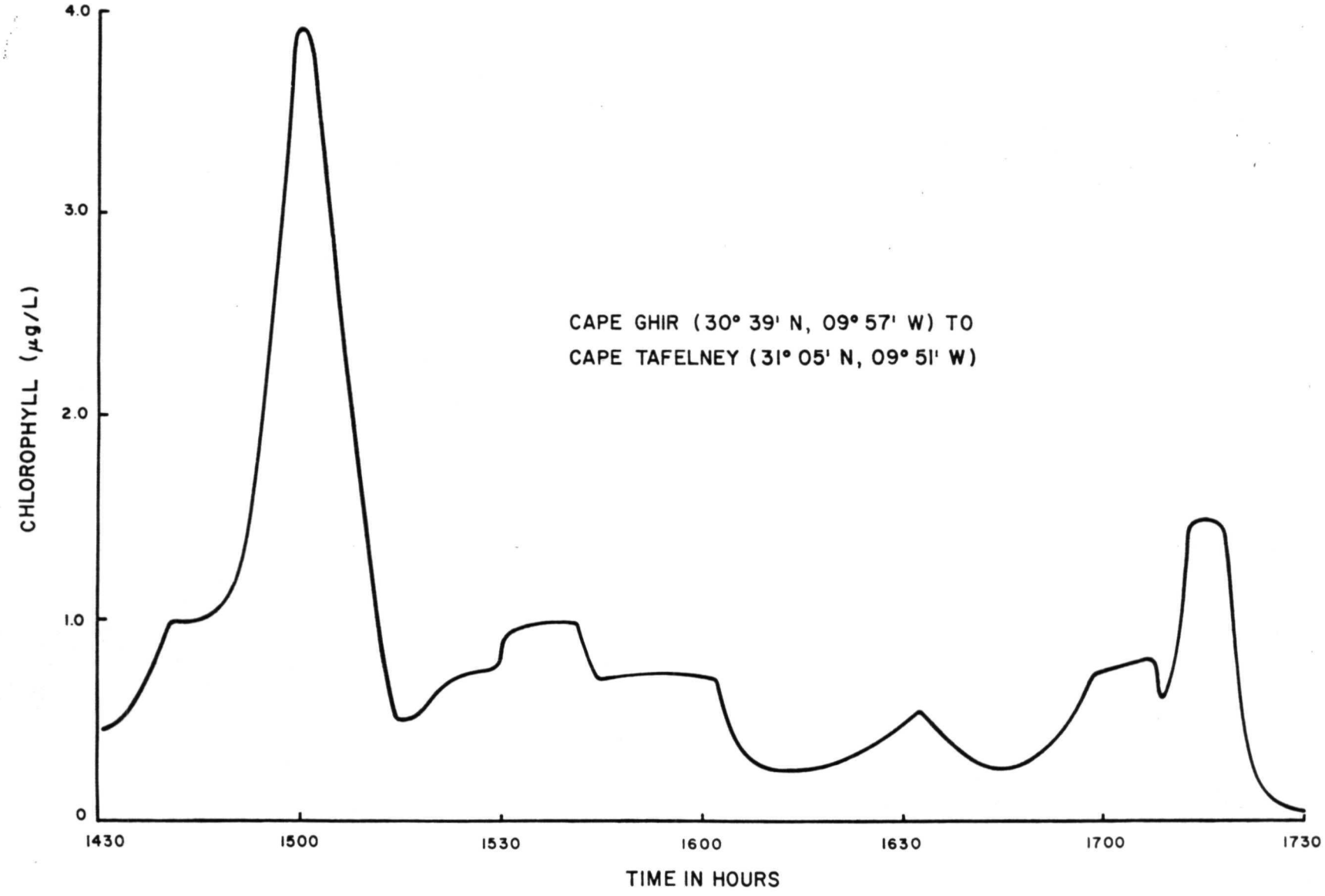
CHLOROPHYLL (µg/L)
4.0
3.0
2.0
1.0
0
CAPE GHIR (30° 39' N, 09° 57' W) TO
CAPE TAFELNEY (31° 05' N, 09° 51' W)
1430
1500
1530
1600
1630
1700
1730
TIME IN HOURS


1W017-00
26AUG72 C N20-05/W016-16 N N20-04/W016-11 MSS 4
W016-301
W016-001
R SUN EL58 AZ103 189-0470-G-1-N-D-2L NASA ERTS E-1034-11004-4 1

Fig. 16

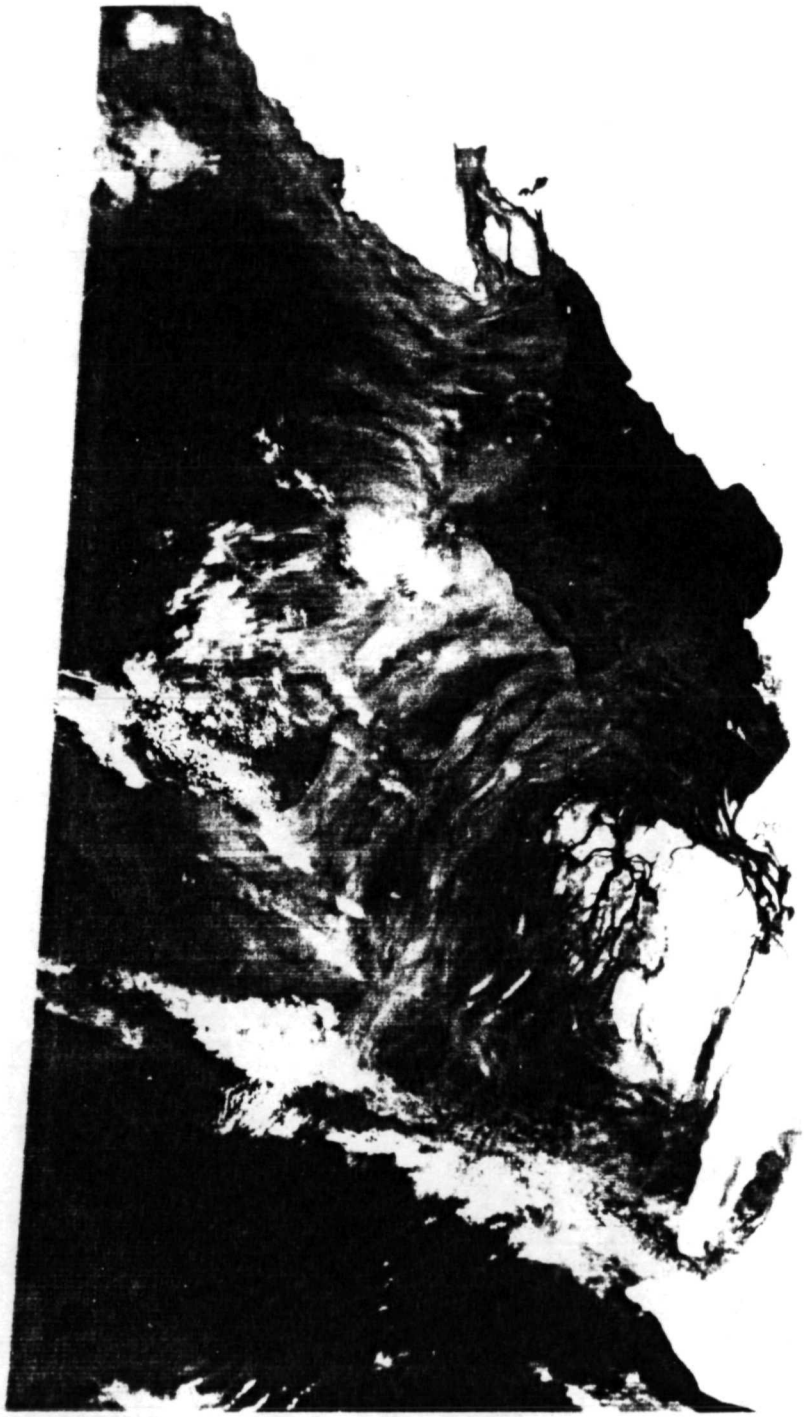

W016-301 W016-001
N20 05/W016-16 N N20-04/W016-11 MSS 5 R SUN EL58 AZ103 189-0470-G-1-N-D-2L NASA ERTS E-1034-11004-5 1

Fig. 17

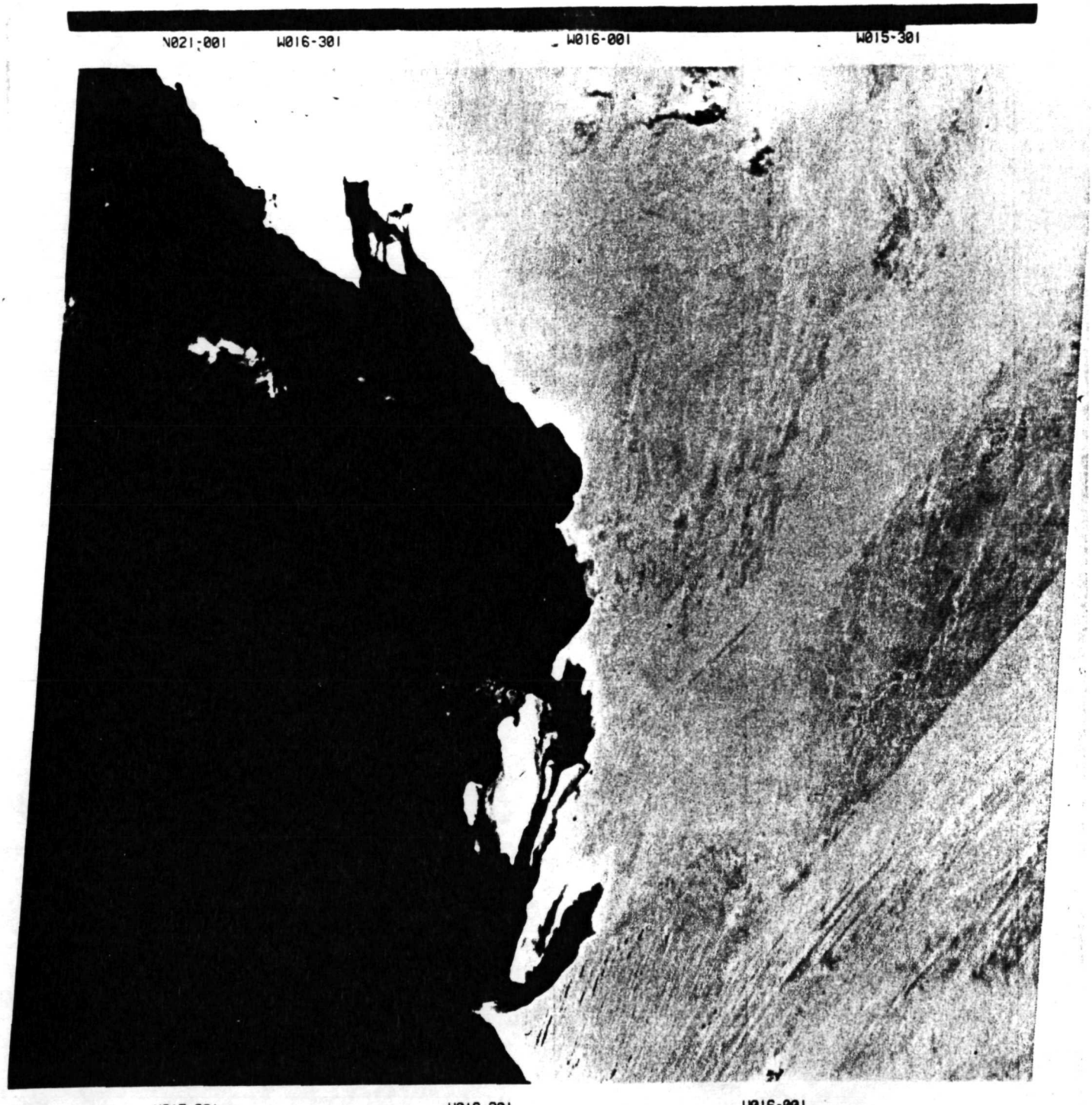
W021-001
W016-301
W016-001
W015-301
W017-001
W016-301
W016-001
06NOV72 C N20-05/W016-16 N N20-02/W016-14 MSS 5 R SUN EL45 AZ141 189-1474-G-1-N-D-2L NASA ERTS E-1106-11012-5 01

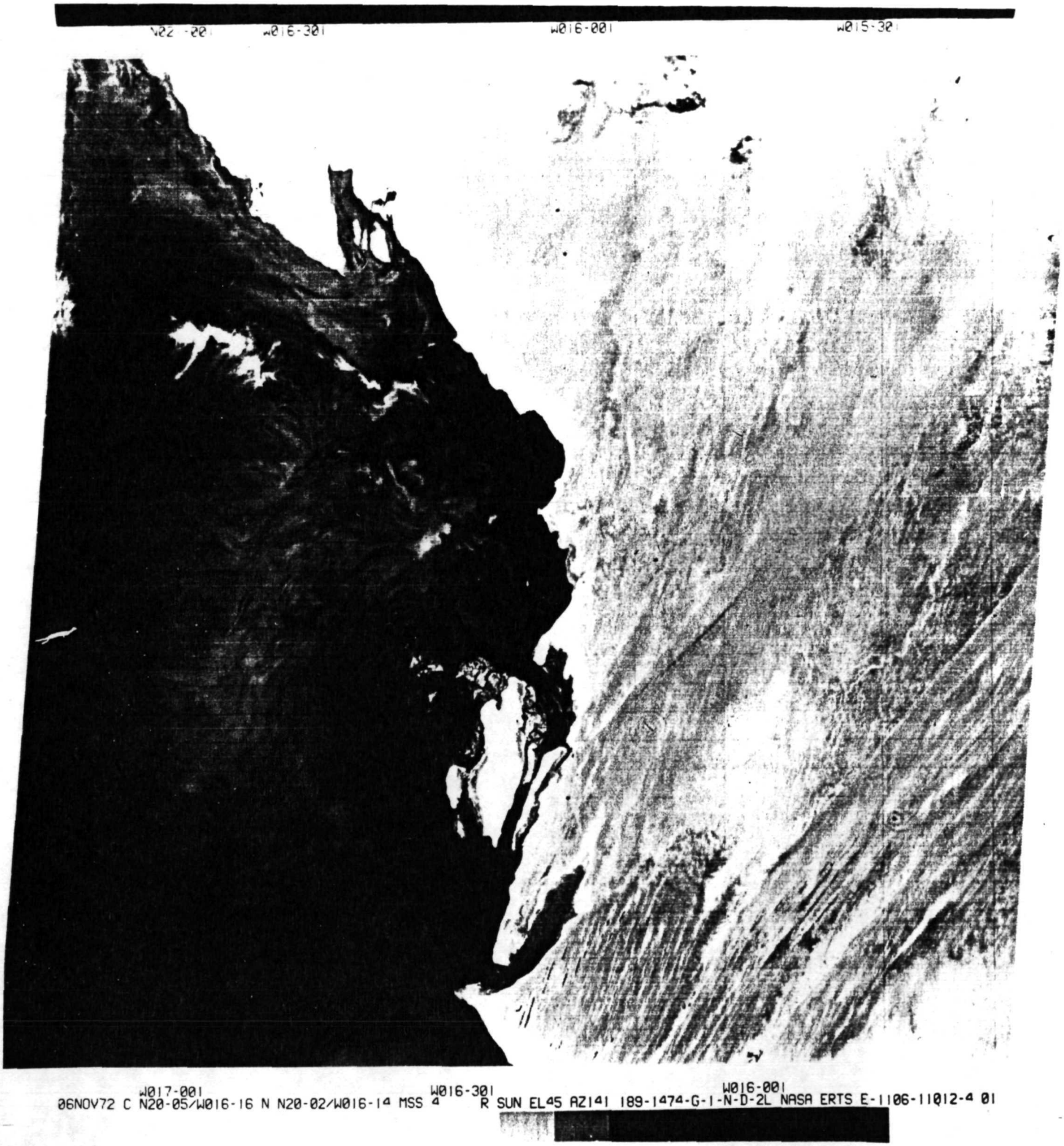
W016-001
W015-30
W017-001
W016-301
W016-001
06NOV72 C N20-05/W016-16 N N20-02/W016-14 MSS 4 R SUN EL45 AZ141 189-1474-G-1-N-D-2L NASA ERTS E-1106-11012-4 01

Fig. 19

W016-301 W016-001 N221-001

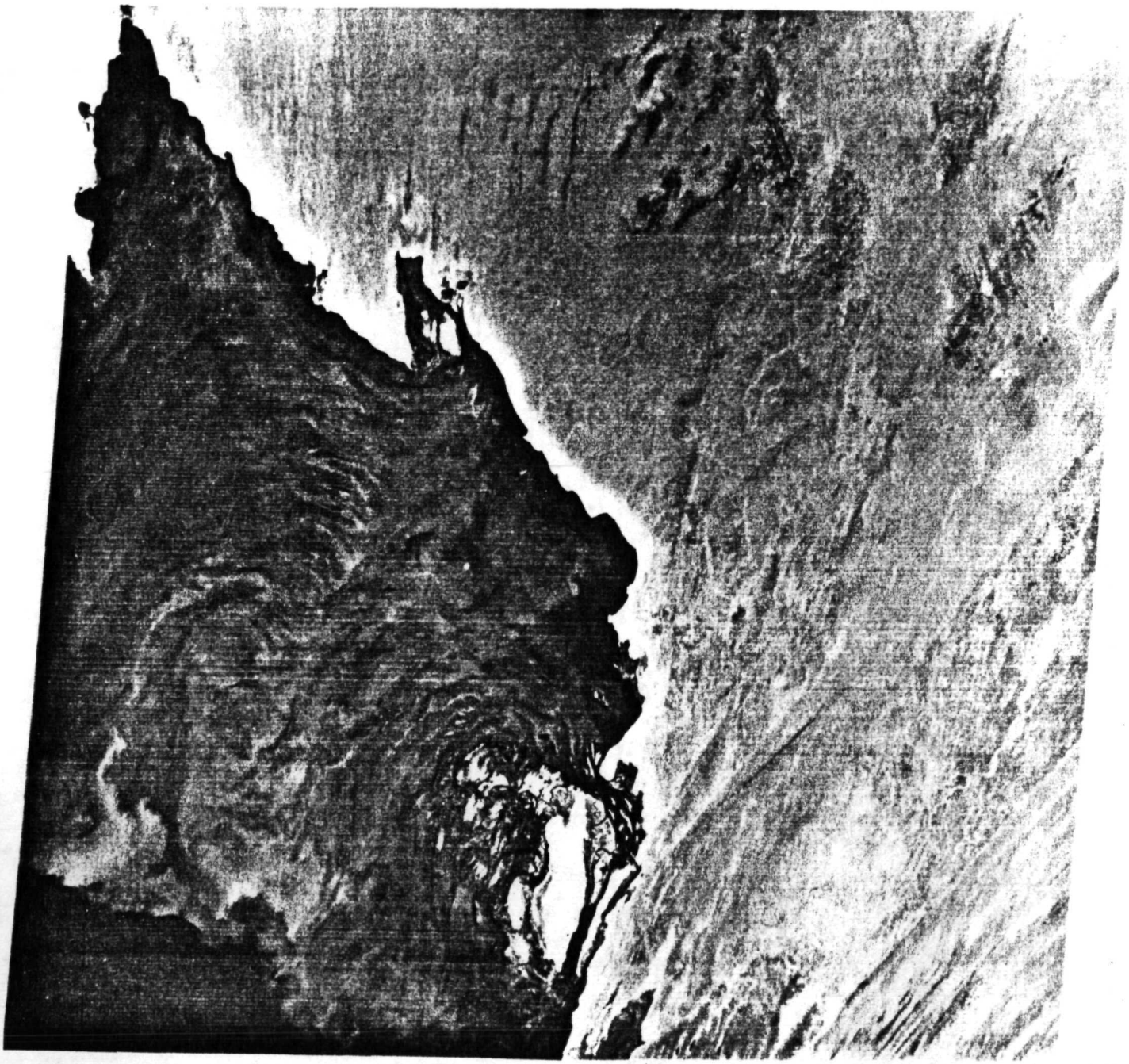

W017-001 IN019-30 W016-301 W016-201
22FEB73 C N20-16/W016-19 N N20-14/W016-15 MSS 4 R SUN EL44 AZ128 189-2980-N-1-N-D-2 214-11014-4 01

FIG. 20

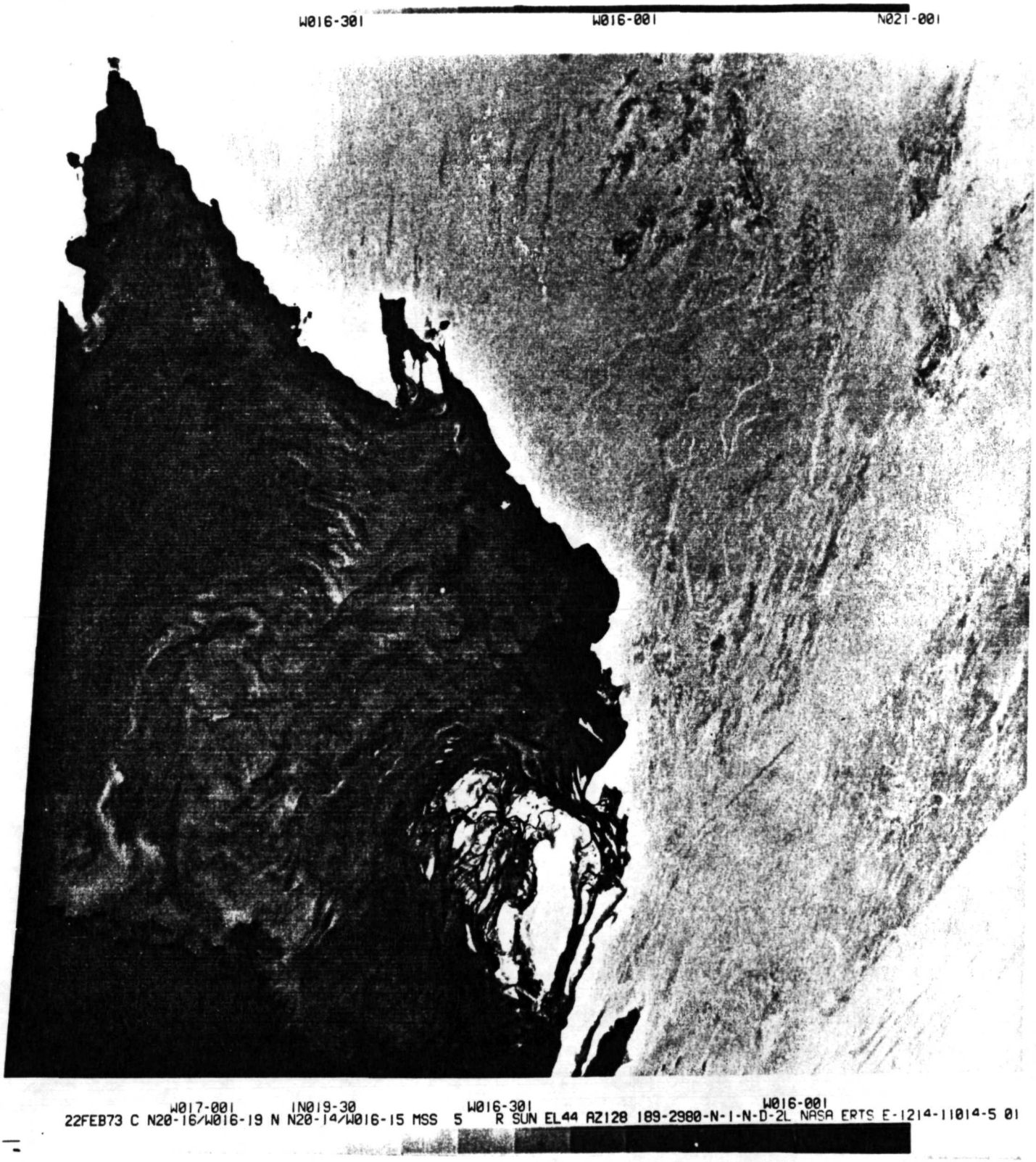
W016-301
W016-001
N021-001
W017-001
IN019-30
W016-301
W016-001
22FEB73 C N20-16/W016-19 N N20-14/W016-15 MSS 5 R SUN EL44 AZ128 189-2980-N-1-N-D-2L NASA ERTS E-1214-11014-5 01

Fig. 21

W016-301 W016-001 N021-001

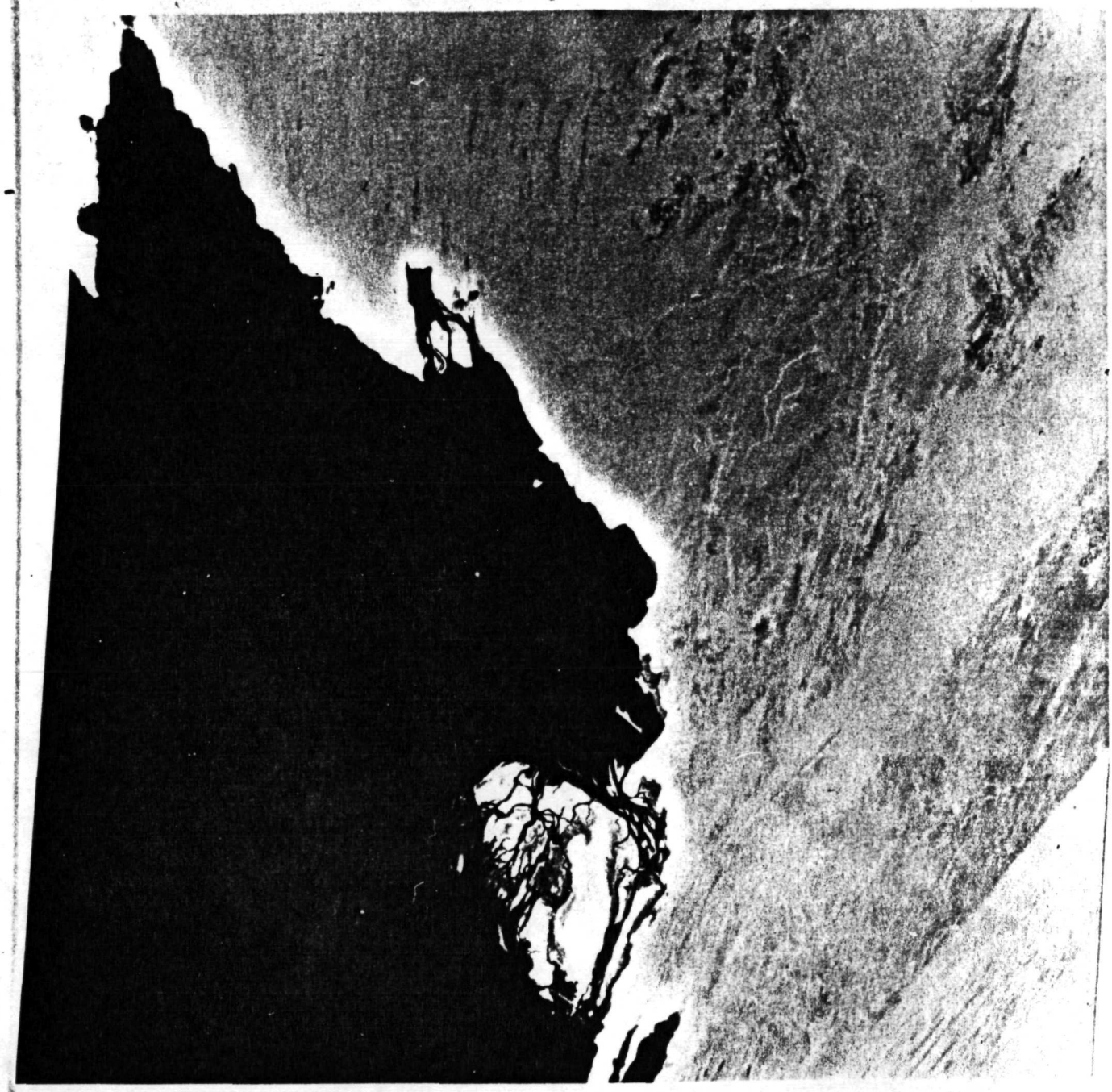

W017-001 IN019-30 W016-301 W016-001
22FEB73 C N20-16/W016-19 N N20-14/W016-15 MSS 6 R SUN EL44 AZ128 189-2980-N-1-N-D-2L NASA ERTS E-1214-11014-6 01

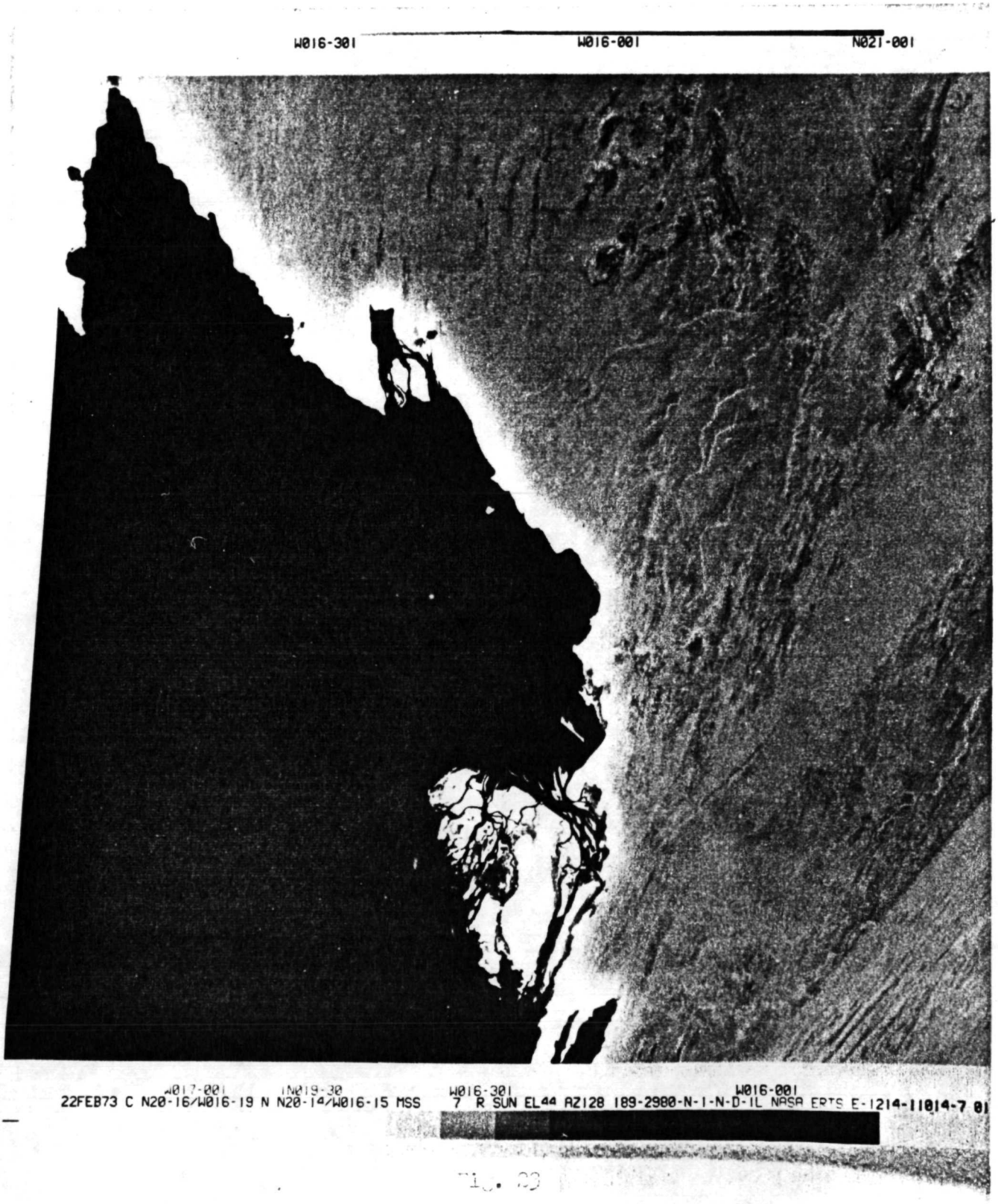
W016-301
W016-001
N021-001
W017-001
N019-30
W016-301
W016-001
22FEB73 C N20-16/W016-19 N N20-14/W016-15 MSS
7 R SUN EL44 AZ128 189-2980-N-1-N-D-1L NASA ERTS E-1214-11014-7 01

Fig. 23

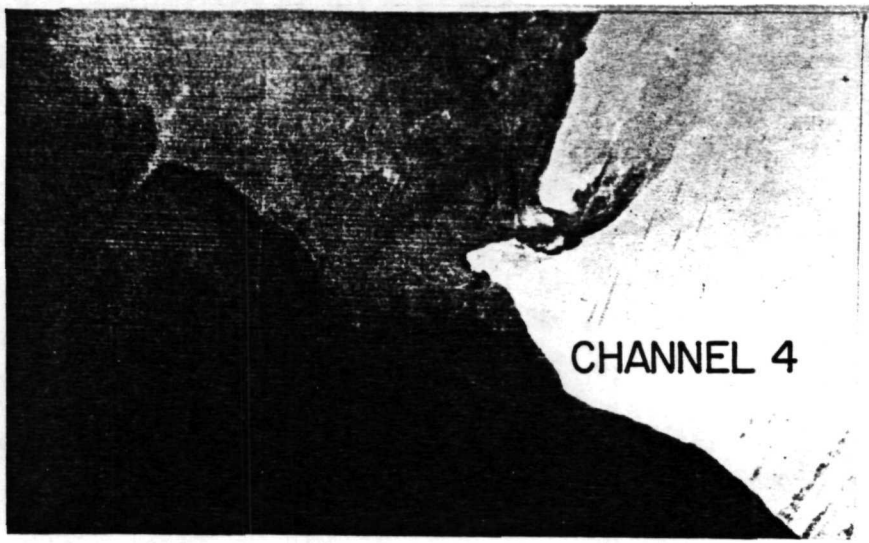

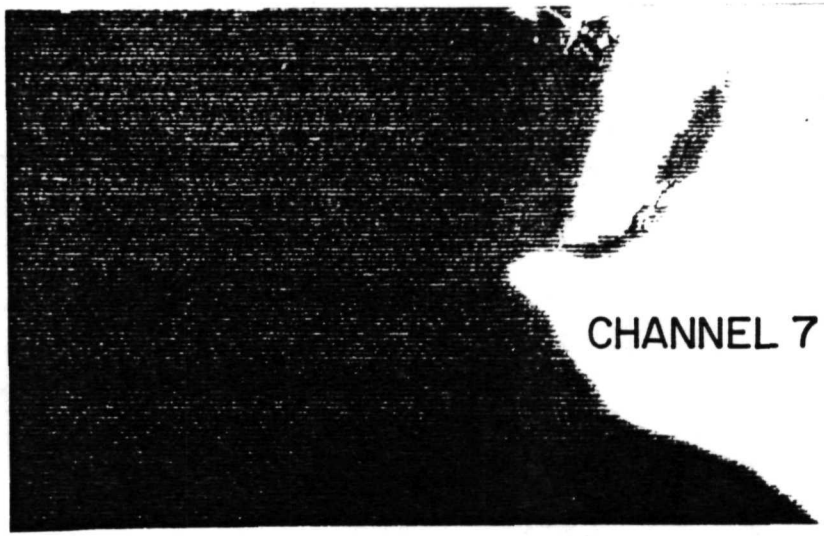

ERTS-1 MSS 1214 - 11020

Fig. 2b

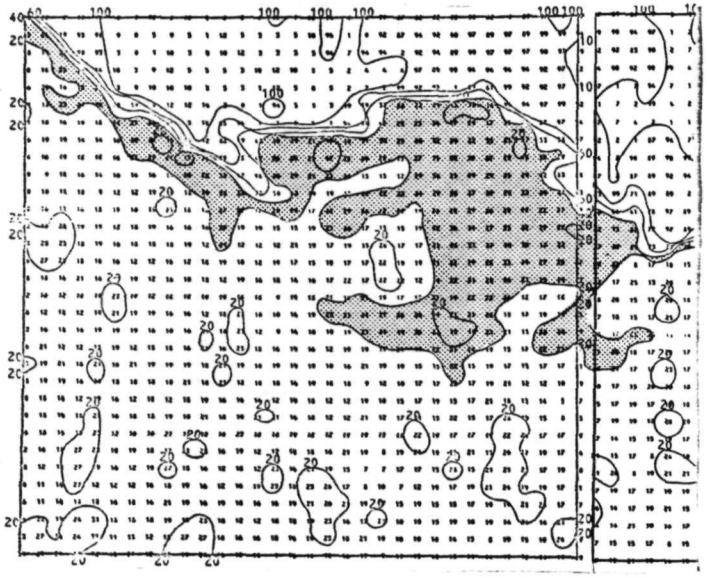

REFLECTED ENERGY

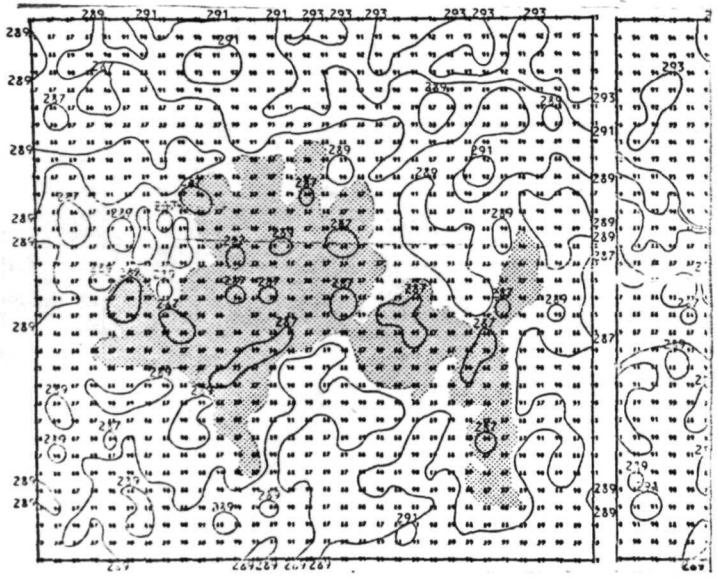

INFRARED RECORDINGS

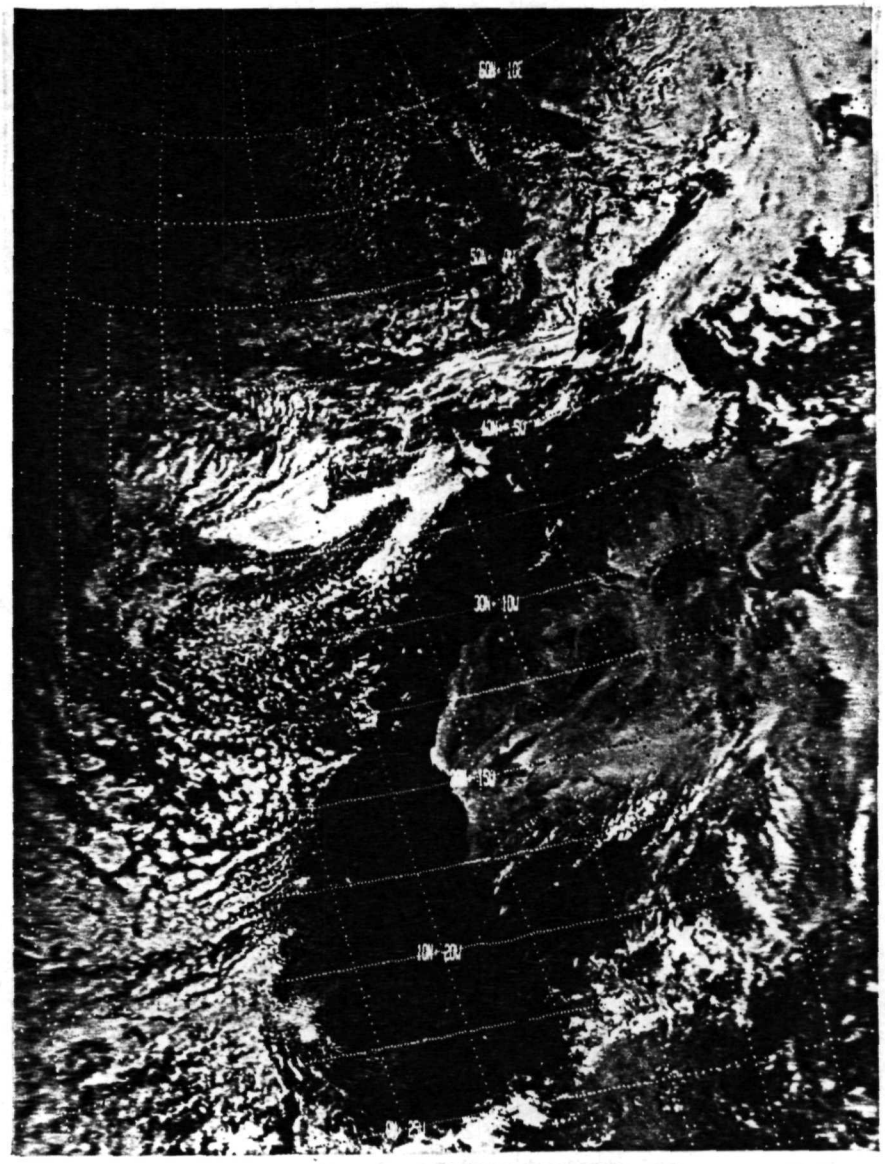

OBSERVATIONS WITH NOAA 2 ON 2 FEBRUARY 1973

Fig. 25

1W017-00 W016-301

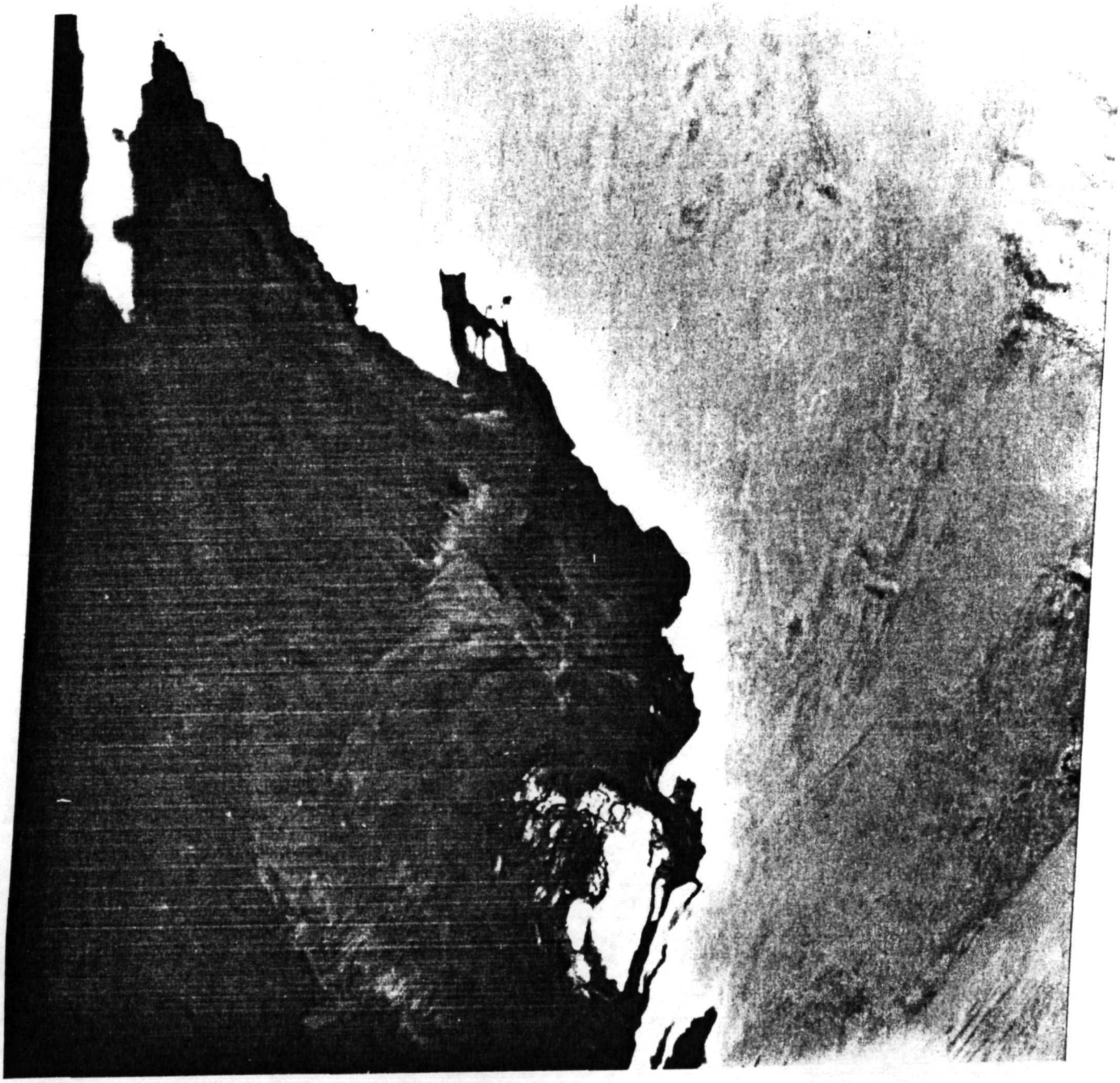

W017-001 1N019-30 W016-301 W016-001
28JUN73 C N20-17/W016-25 N N20-16/W016-19 MSS 5 R SUN EL60 AZ078 188-4737-A-1-N-D-2L NASA ERTS E-1340-11018-5 81

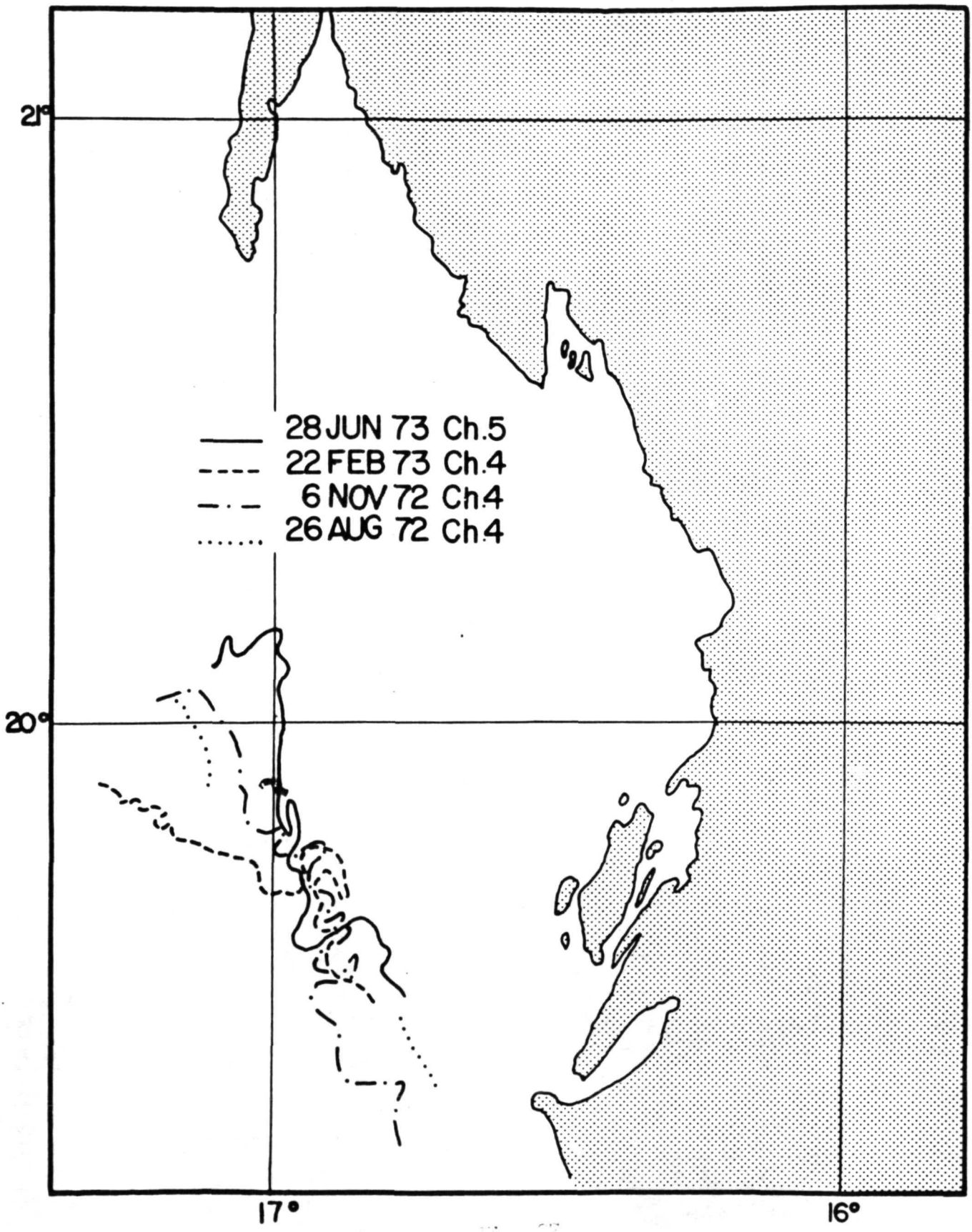
21°
20°
17°
16°
28 JUN 73 Ch.5
22 FEB 73 Ch.4
6 NOV 72 Ch.4
26 AUG 72 Ch.4

22 FEBRUARY 1973
ANALYSIS OF CHANNEL 4 AND 5

FOR DETAILS OF THIS AREA
SEE CHANNELS 6 AND 7

BOUNDARY

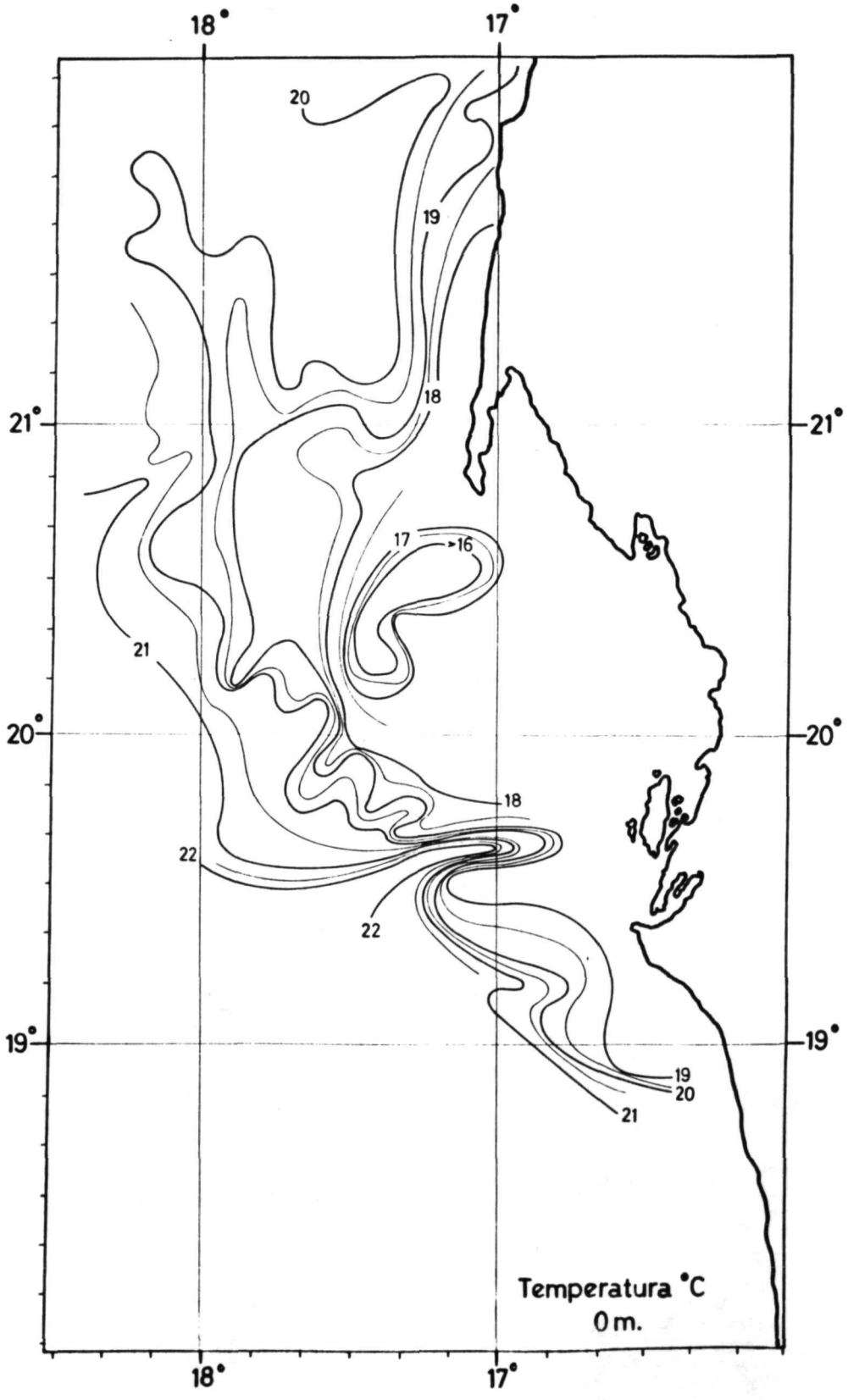

Fig. 09

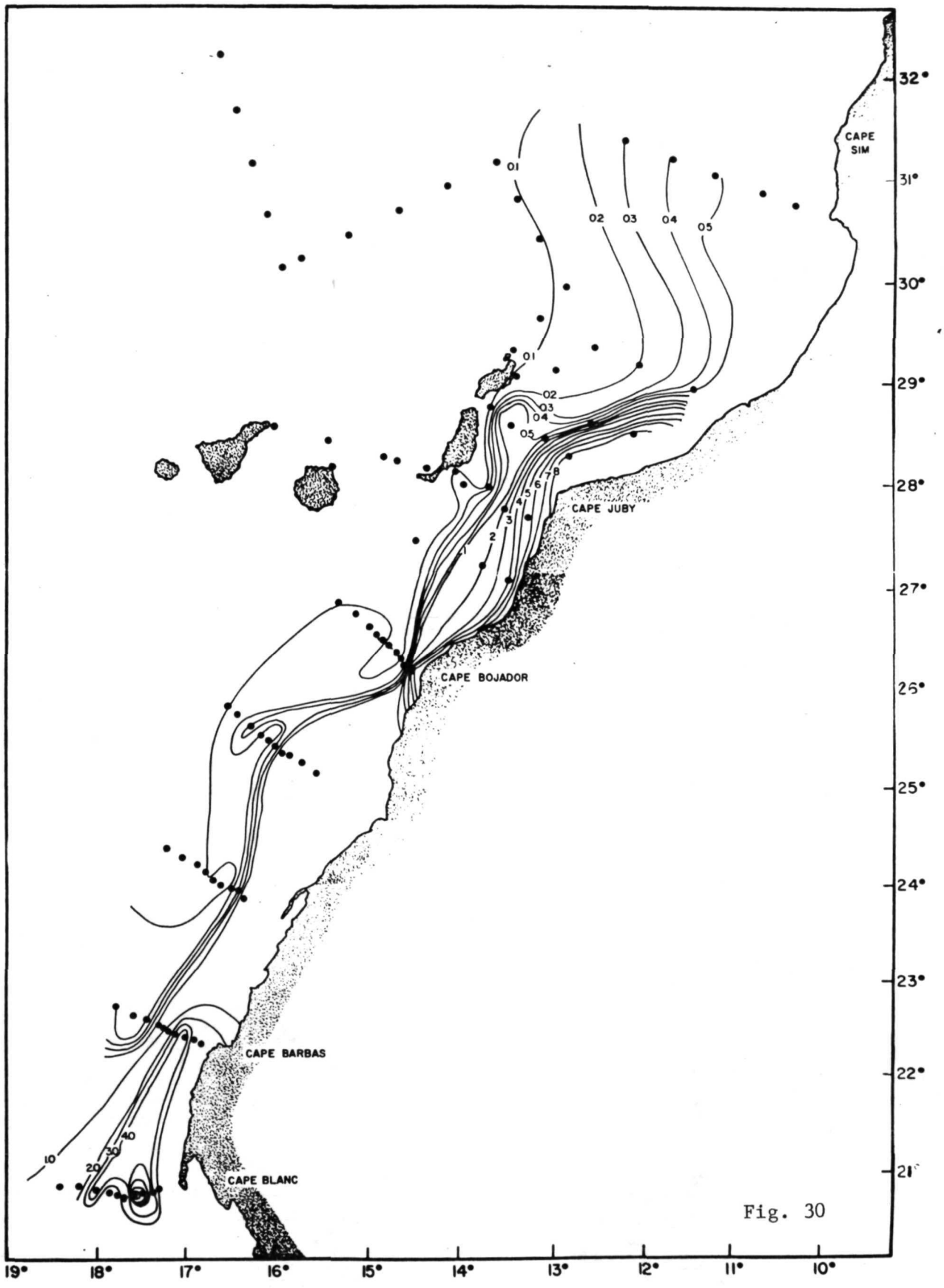
CAPE SIM
CAPE JUBY
CAPE BOJADOR
CAPE BARBAS
CAPE BLANC
01
02
03
04
05
1
2
3
4
5
6
7
8
10
20
30
40
32°
31°
30°
29°
28°
27°
26°
25°
24°
23°
22°
21°
19°
18°
17°
16°
15°
14°
13°
12°
11°
10°

Fig. 30

TOTAL PICTURE SIZE = 585 LINES, 810 SAMPLES/LINE

SECTION 3 OF SEGMENT 2 CHANNEL 4
1033-10524OC 2 4C-A / 4D S1112A07 KEY
25AUG72 C N27-27/W012-53 N N27-25/W012-49
SUR EL57 AZ114 189-0456- -1- D-
NASA ERTS E-1033-10524-

R G-
6B|W013-30M-W013-00|27W012-30||.W012-00| ******** ********
/-HN028-00HH N027-30W36N027-00= ******** ********
11=NC28-007,N027-30=0(N027-00=2 W012-C0= ******** ********
-TW013-30|8P=013-00|Y,N026-30|RZW012-30| ******** ********

FREQUENCY DISTRIBUTION SL= 1 SS= 1 NL= 585 NS= 810 HISTUP= 255 HISTLW= 0

AVERAGE GRAY LEVEL = 64.4413 STANDARD DEVIATION = 12.3571 NUMBER OF POINTS = 473850

FREQUENCY HISTOGRAM - NORMALIZED TO MAXIMUM = 100 (LEVELS WITH ZERO FREQUENCY OMITTED)

GRAY	FREQ	PERCENT
0	364	0.076
2	3	0.000
3	3	0.000
7	1	0.000
8	4	0.000
10	1	0.000
11	3	0.000
12	3	0.000
13	1	0.000
14	3	0.000
15	2	0.000
16	2	0.000
17	1	0.000
18	1	0.000
19	2	0.000
22	1	0.000
23	3	0.000
24	1	0.000
27	1	0.000
29	67	0.014
30	949	0.200
31	1686	0.355
32	5426	1.144
33	7477	1.577
34	9289	1.960
35	6602	1.393
36	1763	0.372
37	3854	0.813
38	2601	0.548
39	3192	0.673
40	2825	0.596
41	2214	0.467
42	1179	0.248
43	563	0.118
44	2227	0.469
45	526	0.111
46	1782	0.376
47	399	0.084
48	546	0.115
49	728	0.153
50	90	0.018
51	263	0.055
52	190	0.040
53	313	0.066
54	788	0.166
55	536	0.113
56	748	0.157
57	948	0.200
58	2843	0.599
59	4655	0.982
60	16694	3.523
61	5146	1.085
62	32784	6.918
63	15640	3.300
64	30775	6.494
65	35779	7.550
66	18638	3.933
67	23703	5.002
68	9401	1.983
69	37141	7.838
70	44671	9.427
71	49631	10.473
72	9979	2.105
73	31927	6.737
74	20412	4.307
75	2055	0.433
76	5215	1.100
77	5459	1.152
78	946	0.199
79	1324	0.279
80	1341	0.283
81	297	0.062
82	512	0.108
83	933	0.196
84	53	0.011
85	162	0.034
86	428	0.090
87	434	0.091
88	127	0.026
89	241	0.050
90	397	0.083
91	234	0.049
93	319	0.067
94	419	0.088
96	153	0.032
97	345	0.072
98	312	0.065
100	221	0.046
101	241	0.050
102	313	0.066
103	243	0.051
104	160	0.033
105	214	0.045
106	138	0.029
107	164	0.034
108	165	0.034
110	20	0.004
111	33	0.006
112	15	0.003
114	1	0.000
123	1	0.000
125	1	0.000
126	7	0.001
128	2	0.000
131	1	0.000
144	1	0.000
148	1	0.000
154	1	0.000
170	1	0.000
194	1	0.000
195	5	0.001
196	1	0.000
197	2	0.000
198	2	0.000
201	2	0.000
202	1	0.000
206	1	0.000
211	2	0.000
213	7	0.001
214	1	0.000
215	1	0.000
217	4	0.000
218	7	0.001
220	3	0.000
221	5	0.001
222	1	0.000
224	1	0.000
230	9	0.001
234	1	0.000
239	1	0.000
240	39	0.008
241	10	0.002
242	12	0.002
243	12	0.002
244	2	0.000
246	1	0.000
247	4	0.000
248	2	0.000
253	1	0.000
255	73	0.015

FIG. 21

```
TOTAL PICTURE SIZE =     585 LINES.     810 SAMPLES/LINE

SECTION     2 OF SEGMENT     2 CHANNEL     4
1033-10524OC 2 4<-A / 4D      SI112407 X<Y
25AUG72 C N27-27/W012-53 N N27-25/W012-49
  SUN EL57 AZ114 189-0456- -1-  D-
 NASA ERTS E-1033-10524-                                  R G-
6@|WC13-30M"W013-00|27WC12-30||.W012-00|  """""""""  """""""""
/+NC28-00=H N027-30=>6N027-00=  """""""""  """""""""  """""""""
II=NC28-007,N027-30=0(N027-00=2 W012-00=  """""""""  """""""""
¬?W013-30|@PW013-00|Y,N026-30|RZW012-30|  """""""""  """""""""

NGRY = 7  GRVAL =   31   33   35   37   39   41   45      GRCHAR =  *8%IO$

START LINE =   1   START SAMPLE =    1   LINE SPACING   12   SAMPLE SPACING   12
```

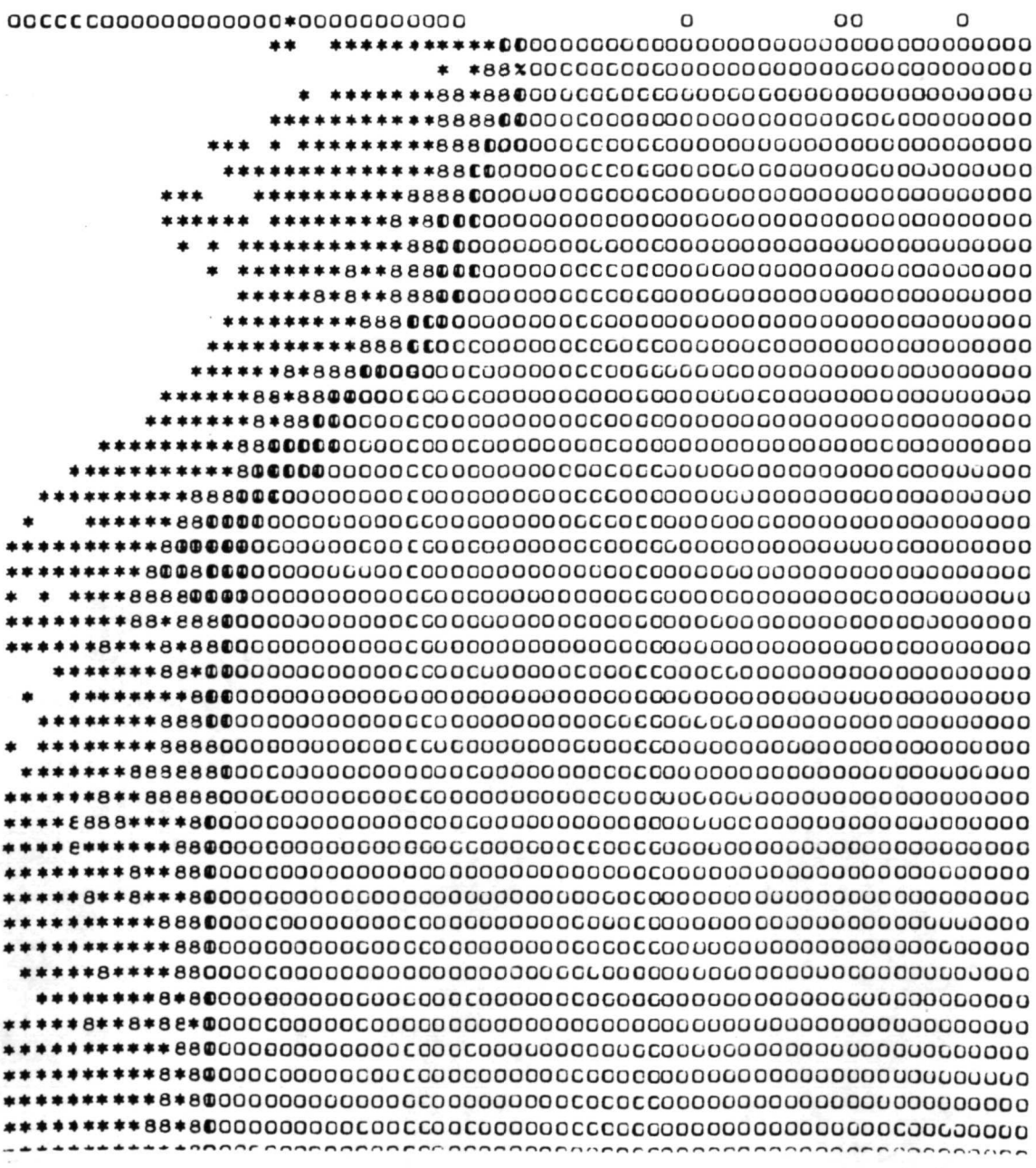

Fig. 22

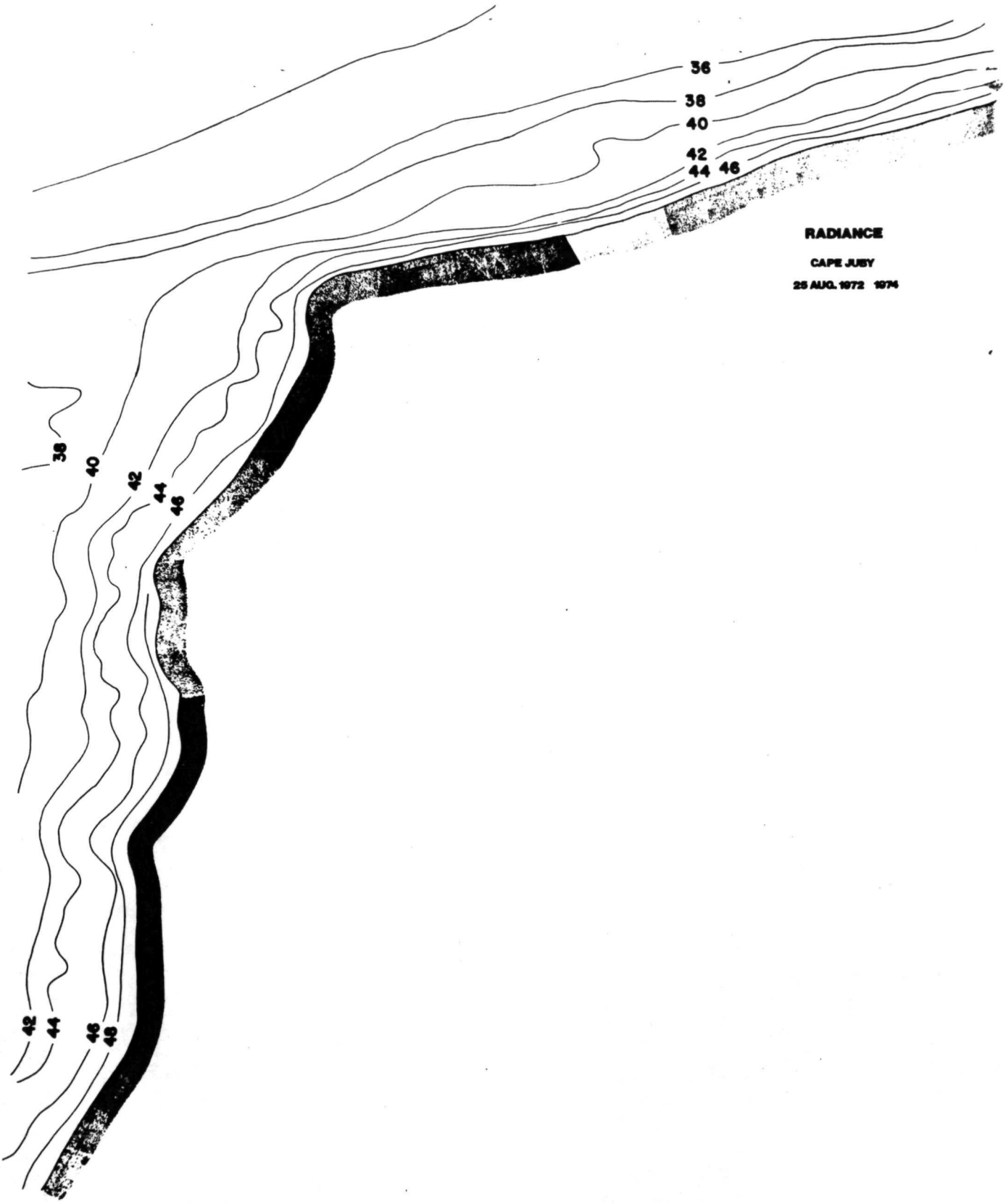
36
38
40
42
44
46
RADIANCE
CAPE JUBY
25 AUG. 1972 1974
38
40
42
44
46
42
44
46
48

Fig. 33

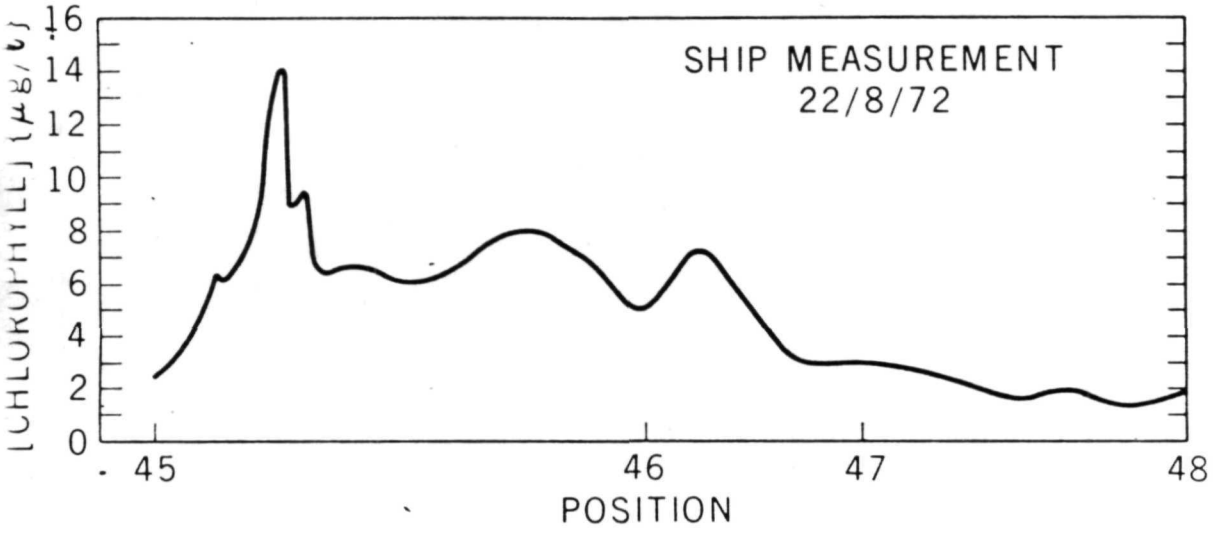
SHIP MEASUREMENT
22/8/72
16
14
12
10
8
6
4
2
0
45
46
47
48
POSITION

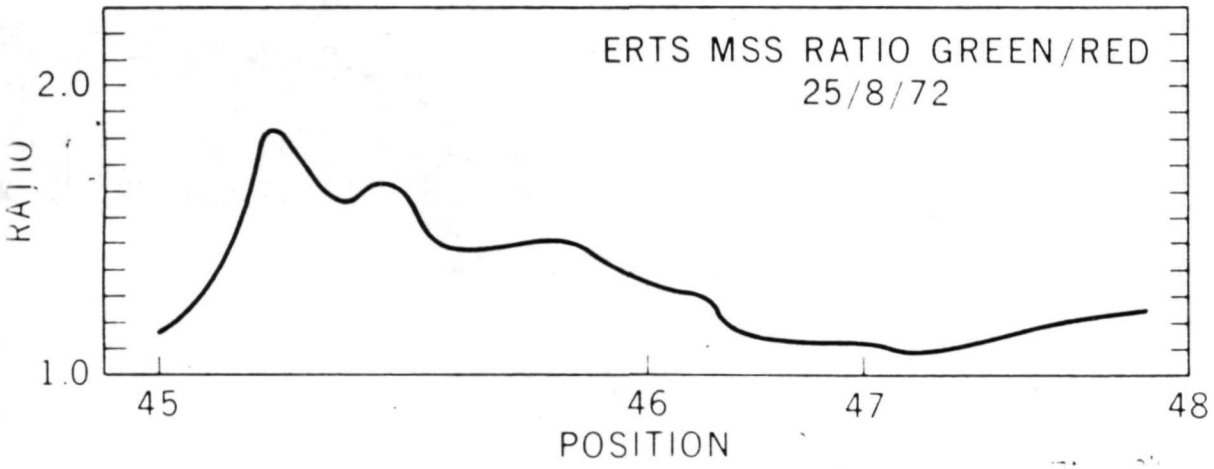
ERTS MSS RATIO GREEN/RED
25/8/72
2.0
1.0
45
46
47
48
POSITION


ERTS-1 MSS-4 λ0.5-0.6 μm
13°30'W
13°00'W
28N
27N
45
47
46

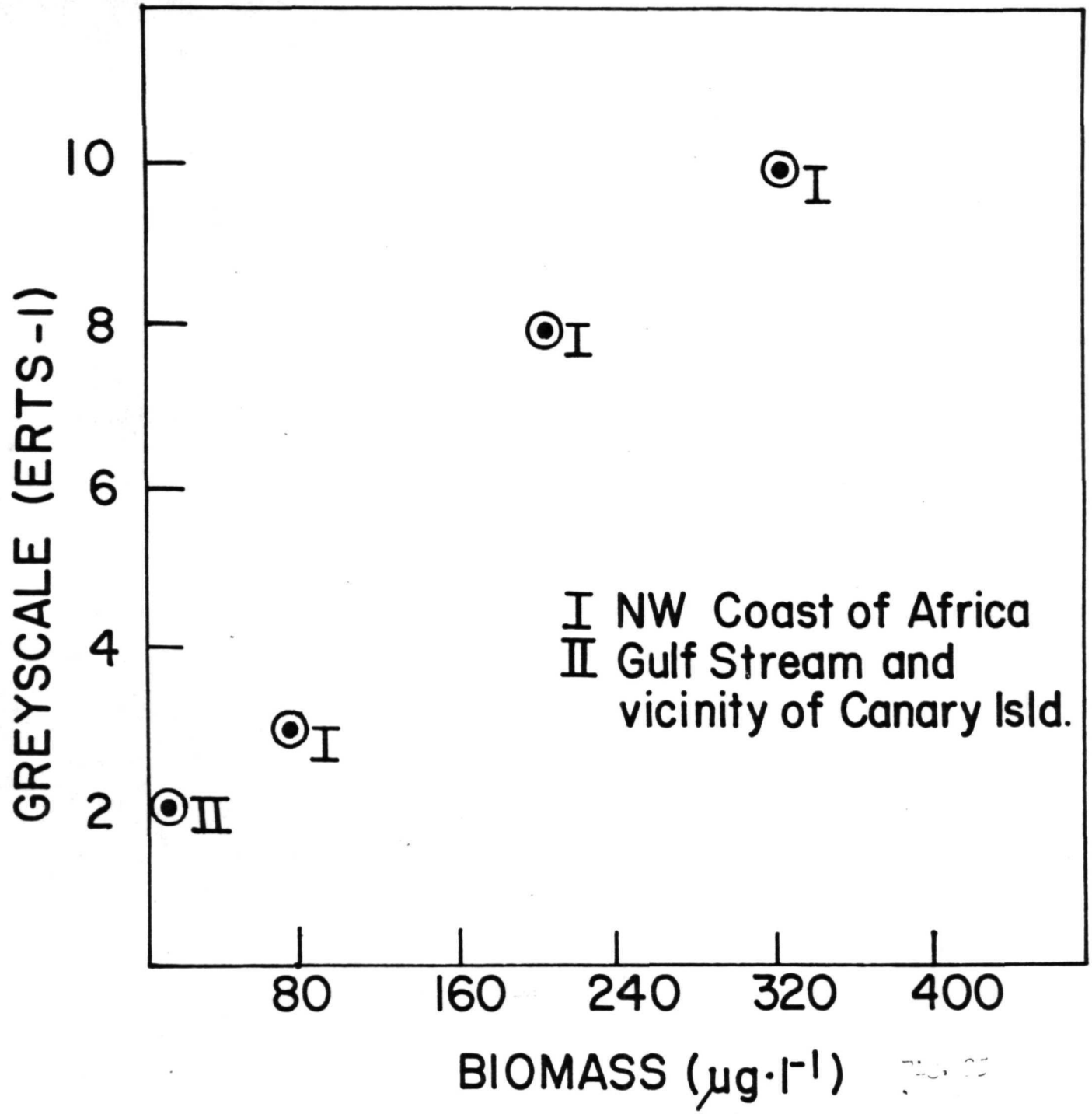
GREYSCALE (ERTS-1)
10
8
6
4
2
I
I
I
II
I NW Coast of Africa
II Gulf Stream and
vicinity of Canary Isld.
80
160
240
320
400
BIOMASS (µg·l⁻¹)

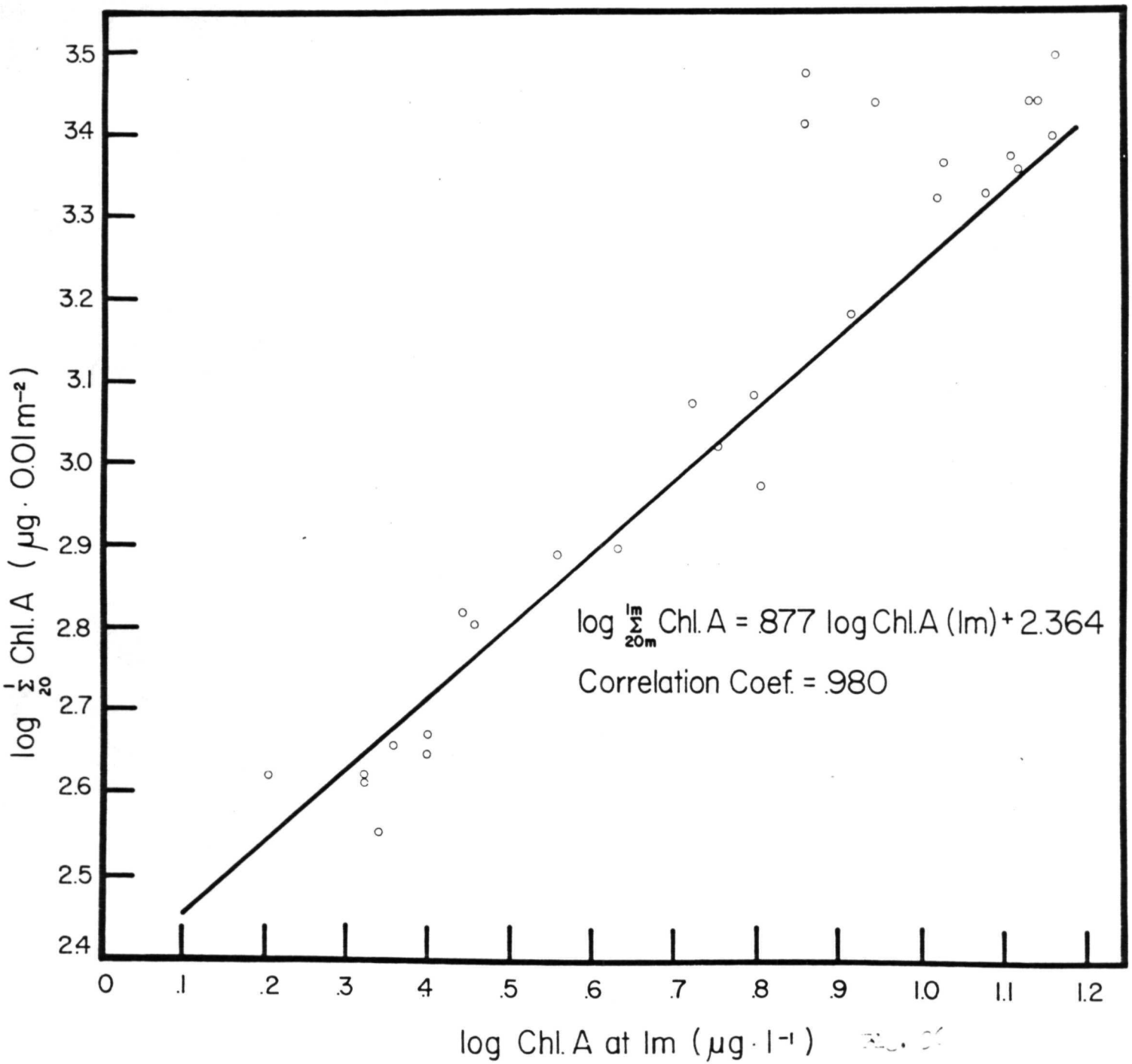
3.5
3.4
3.3
3.2
3.1
3.0
2.9
2.8
2.7
2.6
2.5
2.4
log $\frac{1}{\Sigma}_{20}$ Chl. A (μg · 0.01 m⁻²)
log $\frac{1m}{\Sigma}_{20m}$ Chl. A = .877 log Chl. A (1m) + 2.364
Correlation Coef. = .980
0
.1
.2
.3
.4
.5
.6
.7
.8
.9
1.0
1.1
1.2
log Chl. A at 1m (μg · l⁻¹)